QuNet: Cost vector analysis & multi-path entanglement routing in quantum networks

Hudson Leone,[1,2,*] Nathaniel R. Miller,[3] Deepesh Singh,[4] Nathan K. Langford,[1,2] and Peter P. Rohde[2,3,†]
[1] *School of Mathematical and Physical Sciences, University of Technology Sydney, Ultimo, NSW 2007, Australia*
[2] *Centre for Quantum Software & Information (UTS:QSI), University of Technology Sydney, Ultimo, NSW 2007, Australia*
[3] *Hearne Institute for Theoretical Physics, Department of Physics & Astronomy, Louisiana State University, Baton Rouge LA, United States*
[4] *Centre for Quantum Computation & Communication Technology, School of Mathematics and Physics, The University of Queensland, St Lucia, Queensland 4072, Australia*

Entanglement distribution will form the backbone of many future distributed quantum technologies, especially the quantum internet. The act of purifying multiple noisy entangled states into a single one of higher quality has no analogue in classical networking and as such, this transforms the way in which we will consider future algorithms for routing entanglement. We outline the differences that arise because of this, demonstrate some elementary formalisms for 'multi-path entanglement routing', and discuss the philosophical differences that arise when comparing this regime to conventional digital network theory. We also present a software package, QuNet, that uses novel 'quantum cost-vector analysis' to simulate and benchmark routing in multi-user entanglement networks in a way that is is highly scalable in network size and the number of competing users. Our software accommodates both ground- and space-based networks, and implements efficient multi-user time-optimisation for mitigating congestion when quantum memories are available.

CONTENTS

* leoneht0@gmail.com
† dr.rohde@gmail.com; https://peterrohde.github.io/QuNet

I. INTRODUCTION

In classical networking, communication is carried out via direct transmission of classical information along communication channels, and errors are mitigated through repeat-until-success strategies that transmit redundant information. In quantum networking, the no-cloning theorem prevents arbitrary copying of unknown quantum information, so direct transmission of quantum information is limited in quality and success probability by the intrinsic noise characteristics of the communication channel. However, these no-cloning limitations can be circumvented if quantum information is distributed in the form of known entangled states, which can be used to communicate arbitrary quantum information using repeat-until-success entanglement transmission and quantum teleportation (Bennett *et al.*, 1993). When combined, in addition, with entanglement swapping and entanglement purification, quantum communication links can be extended to arbitrary length with arbitrarily high transmission quality, effectively bypassing the inevitable transmission noise limitations of the quantum channel. Due to these desirable properties, entanglement distribution will be arguably the most essential requirement in a future quantum internet (Rohde, 2021), with significant potential economic benefits facilitating many essential future quantum technologies (Nielsen and Chuang, 2000) such as quantum key distribution (QKD) (Bennett and Brassard, 1984; Ekert, 1991) (see Sec. IX.A), quantum state teleportation (Bennett *et al.*, 1993), and most importantly distributed quantum computing (see Sec. IX.B).

Here we present some formalisms, insights, and algorithmic approaches for how future multi-user quantum entanglement distribution networks might operate, and highlight the significant conceptual differences between how multi-user quantum and digital networks operate, some of which are highly counterintuitive to those coming from classical networking backgrounds. One of the primary distinctions between quantum and classical networks is that entanglement purification enables *multi-path routing*, whereby rather than using a single shortest path for routing we employ multiple redundant paths which are subsequently purified down into a single Bell pair of higher fidelity than allowed by any of the available constituent paths, as per Fig. 1. We present a high-performance software package `QuNet`, which implements these ideas, allowing for efficient benchmarking of large-scale multi-user quantum networks, accommodating for both static (e.g ground based) and dynamic (e.g space-based) networks, as well as temporal routing and optimisation when quantum memories are available.

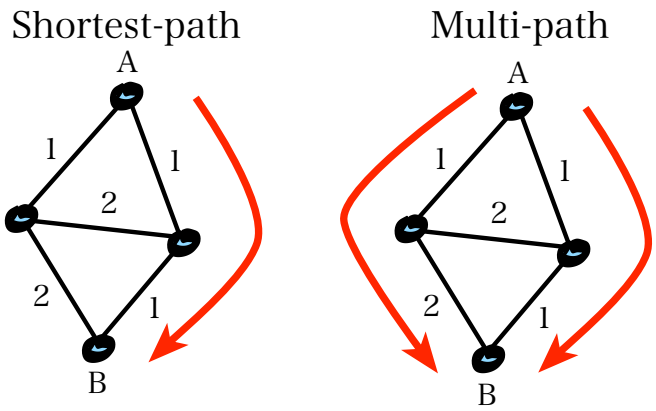

Figure 1: In shortest-path routing, as is often employed in classical networking protocols, we wish to find the route between two nodes that minimises the sum of their edge distances. This notion could similarly be employed in entanglement routing, where the edge weights represent a loss or dephasing noise metric. In multi-path routing, we do not employ just a single shortest-path, but simultaneously communicating Bell pairs across multiple available routes, which are subsequently purified, thereby yielding a single Bell pair with greater fidelity than the shortest-path route would have enabled.

A range of different technologies have been proposed for information distribution and storage in quantum networks approaches based on photonic information distribution including polarisation, time-bin, and spatial mode encoding. Our graph-based network simulation software can be applied in any of these contexts, and extended to include specific details of each (e.g. relevant error mechanisms and network structure properties). So far, our simulations have focused on the context of photonic qubit distribution, but are agnostic to the specific details of information encoding during distribution and storage within the nodes. It seems inevitable that by mere virtue of photons being 'flying qubits' (which propagate at the speed of light), that the future quantum internet will be optically mediated by quantum states of light (Gerry and Knight, 2005). Here there are a multitude of possible mechanisms for encoding quantum information into optical states. For the purposes of our presentation we will primarily refer to examples based upon polarisation-encoded single photons, however the formalism is indeed generally applicable to all manner of quantum communications networks beyond this.

II. ENTANGLEMENT DISTRIBUTION NETWORKS

Suppose our objective is to find the path through a network that is least likely to incur one or more errors in transmitting data. This is a simple matter for a classical network since the dominant error mechanism is loss. We can define weights for each channel based on how likely the channel is to fail at transmitting a bit, and then use any shortest-path algorithm over those weights to find the optimal solution. With quantum networks however, developing a scalar cost for each link is not possible since there are multiple orthogonal error channels, and so the action of an error channel generally depends on the underlying state. Our aim in this section is to implement a formalism that can exploit a similar kind of cost-analysis over entanglement distribution networks. This requires that we consider a simplified error model so as to describe the effects of quantum channels with one or more scalar costs.

We want to describe such networks as generally as possible, so another goal is to use generic tools that apply comprehensively across different varieties and instances of networks. We therefore take a graph theoretic approach for representing networks. Specifically, we model our network as a graph of nodes and communication channels,

$$G = (V, E). \tag{2.1}$$

Here, the graph vertices V represent local nodes, defining end-users, or devices that implement quantum operations (such as entanglement sources, swappers or routers), and edges E between vertices represent quantum communication channels.

A. Bell pairs — A resource for quantum networking

In entanglement distribution networks, entangled states represent the fundamental underlying resource we wish to utilise. For qubit-based networks, the archetypal entangled states are the maximally entangled Bell states between a pair of qubits,

$$\begin{aligned} |\Phi^{\pm}\rangle_{A,B} &= \frac{1}{\sqrt{2}}(|0\rangle_A |1\rangle_B \pm |1\rangle_A |0\rangle_B), \\ |\Psi^{\pm}\rangle_{A,B} &= \frac{1}{\sqrt{2}}(|0\rangle_A |0\rangle_B \pm |1\rangle_A |1\rangle_B). \end{aligned} \tag{2.2}$$

These become the basic resource for all operations in the network. The four states are equivalent as entanglement resources and provide the same utility for elementary network operations. As a known resource state, these Bell pairs are not subject to the no-cloning limitation. Bell pairs also have the useful property that Pauli errors commute across the the qubits of an entangled pair, meaning that an error on one qubit can be equivalently taken to mean an error on the other qubit (up to global phase),

$$(\hat{\sigma} \otimes \hat{I}) |\psi\rangle \propto (\hat{I} \otimes \hat{\sigma}) |\psi\rangle, \tag{2.3}$$

where $\hat{\sigma} \in \{\hat{X}, \hat{Y}, \hat{Z}\}$ and $|\psi\rangle \in \{|\Phi^{\pm}\rangle, \{|\Psi^{\pm}\rangle\}$.

B. Quantum channels

In describing our quantum channels, we take an approach that naturally adapts the cost analysis of classical networking to the regime of quantum networks. Specifically, our channels are weighted with vectors of additive costs that characterise the accumulation of noise as qubits traverse network paths. Although we focus here primarily on *physical* cost mechanisms, such as decoherence and loss, the formalism we present can also be extended to non-physical costs, such as monetary cost.

1. General quantum channels

We consider physical quantum error channels of the form,

$$\mathcal{E}(\hat{\rho}) = p\hat{\rho} + (1-p)\hat{\rho}_{\text{ss}}, \tag{2.4}$$

where $\hat{\rho}_{\text{ss}}$ is the steady state of the channel, satisfying,

$$\mathcal{E}(\hat{\rho}_{\text{ss}}) = \hat{\rho}_{\text{ss}}. \tag{2.5}$$

This means the channel has some probability to transmit the encoded information successfully, and some probability to replace it with the steady state of the channel. Under repeated applications of the channel, we find that the success probability scales exponentially with the number of repetitions n,

$$\mathcal{E}^n(\hat{\rho}) = p^n\hat{\rho} + (1-p^n)\,\hat{\rho}_{\text{ss}}. \tag{2.6}$$

Likewise, a sequence of channels of the same type (i.e. dephasing, depolarising, etc.) but with different success probabilities give rise to the aggregate error channel,

$$\mathcal{E}_{(n)} \circ \cdots \circ \mathcal{E}_{(1)}(\hat{\rho}) = \left(\prod_{i=1}^{n} p_i\right)\hat{\rho} + \left(1 - \prod_{i=1}^{n} p_i\right)\hat{\rho}_{\text{ss}}, \tag{2.7}$$

Thus, under the right circumstances, we see that $-\log(p)$ can be used as an additive cost for a particular type of error across a quantum network. In the next sections, we define the specific channels for several of the most common decoherence and loss errors.

2. Loss channels

The loss channel is a very important effect in any quantum network, especially photonic quantum networks. For a single-qubit state $\hat{\rho}$, it is defined as,

$$\mathcal{E}_{\text{loss}}(\hat{\rho}) = \eta\hat{\rho} + (1-\eta)\,|vac\rangle\langle vac|, \tag{2.8}$$

where η is the transmission efficiency and $|vac\rangle$ denotes the vacuum state. This channel naturally takes the form of Eq. 2.4, with the channel success probability $p = \eta$ and the vacuum as the steady state $\hat{\rho}_{\rm ss} = |vac\rangle\langle vac|$.

3. Decoherence channels

The most commonly studied types of decoherence channels are the dephasing channel,

$$\mathcal{E}_{\rm deph}(\hat{\rho}) = p_{\rm deph}\,\hat{\rho} + (1 - p_{\rm deph})\left[\frac{\hat{\rho} + \hat{Z}\hat{\rho}\hat{Z}}{2}\right], \qquad (2.9)$$

where the steady state is the maximally dephased state $(\hat{\rho} + \hat{Z}\hat{\rho}\hat{Z})/2$; the depolarising channel,

$$\mathcal{E}_{\rm depol}(\hat{\rho}) = p_{\rm depol}\,\hat{\rho} + (1 - p_{\rm depol})\,\frac{\hat{\mathbb{I}}}{2}, \qquad (2.10)$$

where the steady state is the maximally mixed state $\hat{\mathbb{I}}/2$; and the energy decay or amplitude damping channel,

$$\mathcal{E}_{\rm damp}(\hat{\rho}) = p_{\rm damp}\,\hat{\rho} + (1 - p_{\rm damp})\,|0\rangle\langle 0|\,, \qquad (2.11)$$

which arises very naturally in the context of atom-like qubits, where the finite energy gap causes all states to decay towards a steady state of the ground state, which encodes the logical '0' state.

For the dephasing channel, it is often parameterized differently as a pure phase-flip process (Nielsen and Chuang, 2000),

$$\mathcal{E}_{\rm deph}(\hat{\rho}) = \left(\frac{1 + p_{\rm deph}}{2}\right)\hat{\rho} + \left(\frac{1 - p_{\rm deph}}{2}\right)\hat{Z}\hat{\rho}\hat{Z}. \qquad (2.12)$$

For certain special cases, such as when a dephasing channel is applied to one half of a maximally entangled Bell state, the error state defined in this way, $\hat{Z}\hat{\rho}\hat{Z}$, is orthogonal to the input state, $\hat{\rho}$, and we can directly identify $p_{\rm deph}$ as the overlap probability between the input and output states.

While `QuNet`'s formalism can be used for a wide range of error channels that can be written in the above form, for illustration in the remainder of this paper, we will consider a common scenario where quantum networks are affected by loss and dephasing (Rohde and Ralph, 2006).

4. State fidelity and channel cost-vectors

While quantum channels may be described quite generally in the form of Eq. 2.4, this is not how the quality of shared states is usually characterised. One of the most common metrics used for this purpose is the fidelity, which measures of overlap between the input (or target) state and the transmitted state,

$$F = \langle\psi|\,\mathcal{E}(|\psi\rangle\langle\psi|)\,|\psi\rangle\,. \qquad (2.13)$$

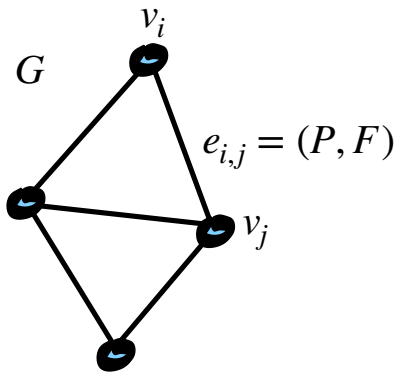

Figure 2: Graph representation for an entanglement distribution network, where a graph G, specified by a set of vertices v_i, and edges $e_{i,j}$. Edges represent the communication of noisy Bell pairs (one pair per edge), each characterised by both their own preparation probability P and fidelity F.

In the case of dephasing, Eq. 2.12 highlights that this fidelity can be directly related to the channel success probability via $F = (1+p_{\rm deph})/2$, in cases like the sharing of entangled Bell pairs that we consider throughout the majority of this paper.

In practice, it is useful to separate measures of state degradation into components associated with decoherence and loss. Then we can define the fidelity conditional upon no loss, and the probability of no loss as,

$$F_{\rm cond} = \frac{\langle\psi|\,\mathcal{E}(|\psi\rangle\langle\psi|)\,|\psi\rangle}{\eta},$$
$$\eta = 1 - \langle vac|\,\mathcal{E}(|\psi\rangle\langle\psi|)\,|vac\rangle\,. \qquad (2.14)$$

In terms of the generic quantum channels above, this approach can be understood in terms of conditional success probabilities. For example, for a channel with both loss and dephasing, we can define an overall channel success probability,

$$p_{\rm overall} = p_{\rm deph\ |\ (no\ loss)} \times p_{\rm (no\ loss)}, \qquad (2.15)$$

where $p_{\rm (no\ loss)} = \eta$.

Clearly, efficiency and conditional fidelity are in some sense "orthogonal". They are independent measures that characterise two different phenomena of quantum error channels. The former is attributed to amplitude while the latter is of orientation with respect to the ideal state. It is helpful therefore to consider each link in our quantum network in terms of a "cost-vector" that contains the expected efficiency and conditional fidelity for a qubit that passes through it,

$$e = (\eta, F), \qquad (2.16)$$

From this point on, every mention of fidelity will be understood to mean the conditional fidelity as defined in Eq. 2.14, unless stated otherwise. In the following sections, we describe two key primitive processes of entanglement

distribution quantum networking—entanglement swapping and purification—and how to track them within our cost vector formalism.

C. Cost vector analysis in entanglement swapping networks

Having defined the costs and error processes associated with individual quantum links, we now develop the tools required to aggregate the costs for a path in the network. Eq. 2.7 describes a state after it is sent through a special-case sequence of quantum channels. In this case, we find that $-\log(p)$ can be used as an additive cost for the individual links. For entanglement distribution networks however, the constituent qubits of entangled states are often transmitted along separate channels. Fortunately, for the distribution of Bell pairs, we find that the same simple result holds, which results from the symmetry of the state. Specifically, we refer to Eq. 2.3 which demonstrates that Pauli errors commute across the qubits of an entangled pair.

It remains to be shown however that entanglement swapping—perhaps the most important operation in quantum networking—obeys the relation of Eq. 2.7. Entanglement swapping is an operation where two halves of distinct entangled pairs are taken and measured in the Bell basis. This projects entanglement across the outer two qubits, which are never physically interacted, and creates a longer range entangled pair at the cost of two shorter ones. A schematic of this operation is illustrated in Fig. 3. Importantly, the specific order in which entanglement swapping operations are carried out to distribute entanglement across the ends of a network path has no bearing on the success probability of transmitting the state. Because our primary interest is to develop a cost formalism in terms of this probability, we neglect the logistics of distributing entanglement and only consider the costs of doing so.

It is intuitively demonstrated that entanglement swapping has the effect of accumulating the Pauli errors of the constituent Bell states, which allows us to represent the processes within our cost-vector formalism. First, we can always assume that the inner two qubits of the swapping procedure are ideal given that any Pauli errors may be commuted to the outer qubits of the Bell pair. If the projective measurement is assumed to be ideal, then clearly the resulting state will inherit the errors accumulated on the outer two qubits. Additionally, any non-ideal measurement can be represented as an ideal measurement followed by some error channel, and so our cost-vector approach is consistent for all swapping scenarios.

Entanglement swapping can be performed deterministically using a CNOT gate, or non-deterministically in the photonic context using a polarising beamsplitter (PBS), which implements a partial Bell measurement and is only able to resolve two of the four Bell states (Pan *et al.*, 1998). Whether or not an entanglement swapping operation is deterministic has no bearing on the underlying cost-vector formalism, since any non-deterministic effect can be built into the cost.

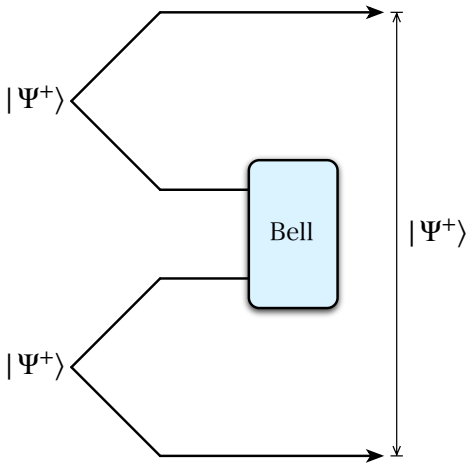

Figure 3: Entanglement swapping of two Bell-pairs, using a Bell measurement between one half of each, to project the remaining two qubits, which were not previously entangled, into a Bell-pair.

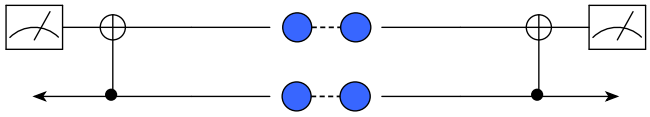

Figure 4: Entanglement purification of two noisy Bell-pairs under dephasing channels, using two CNOT gates.

D. Cost-vector analysis with entanglement purification

The second key ingredient in entanglement distribution networks is entanglement purification, whereby two low-fidelity Bell pairs are reduced into a single higher-fidelity one. This process can be applied recursively so as to achieve arbitrarily high fidelities in principle. However, given that each application of the protocol reduces two Bell-pairs to one, the number of Bell-pair resource states required to apply n rounds of purification scales as 2^n.

As with entanglement swapping, entanglement purification can be implemented using CNOT gates, as shown in Fig. 4, or optically using polarizing beamsplitters (PBSs), as shown in Fig. 5, which comes at the cost of non-deterministic operations similar to PBS-based Bell measurements.

We remarked earlier in Sec. II.B.4 that any state can be described in terms of a "cost-vector" of efficiency and fidelity with respect to some ideal. One reason why this is useful is that cost-vectors of input states can be used to calculate the cost-vector of a purification scheme. For

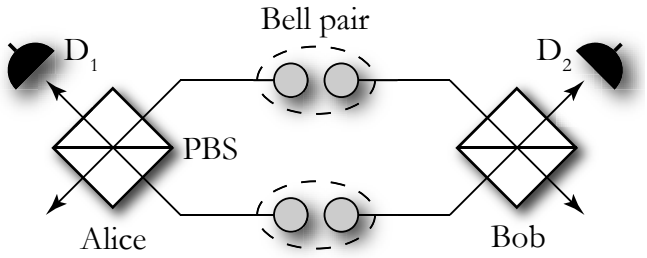

Figure 5: Entanglement purification of two noisy Bell-pairs under dephasing channels, using two polarising beamsplitters (PBS), which implement partial Bell-state projections.

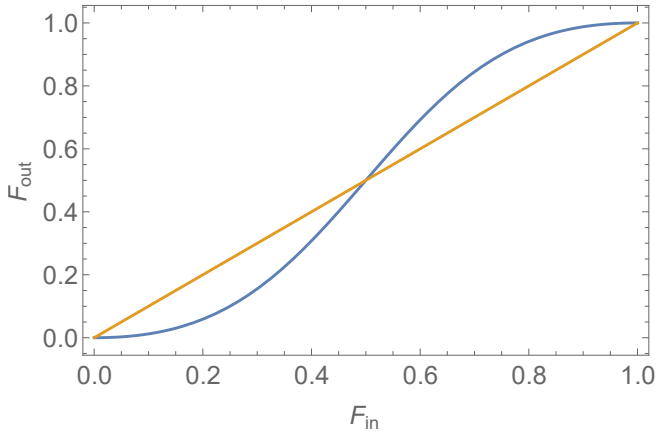

Figure 6: Input versus output fidelities for the entanglement purification protocol shown in Fig. 5, where both input Bell states are assumed to be identical with fidelity F_{in}. So long as $F_{\text{in}} > \frac{1}{2}$, the protocol increases the output fidelity, $F_{\text{out}} > F_{\text{in}}$.

this paper, we consider the photonic implementation of purification as shown in Fig. 5 with the following transformation rules (Jian-Wei *et al.*, 2001):

$$F' = \frac{F_1 F_2}{F_1 F_2 + (1-F_1)(1-F_2)},$$
$$\eta' = \eta_1 \eta_2 [F_1 F_2 + (1-F_1)(1-F_2)], \tag{2.17}$$

F_i and P_i denote the fidelity and probability of the two input Bell-pairs, where $i \in \{1, 2\}$. This relationship is shown in Fig. 6. The protocol has the property that so long as both input Bell-pairs satisfy $F > \frac{1}{2}$, the fidelity of the output Bell-pair will be greater than that of both input pairs,

$$F' > F_1, F_2 \ \forall \ F_1, F_2 > \frac{1}{2}. \tag{2.18}$$

III. GRAPH REDUCTION

Given a large network graph it can be useful to reduce the overall complexity of the graph topology using graph reduction rules that arise from the graph transformations implemented by elementary operations such as swappers and purification.

For example, a linear chain of entanglement swappers has the effect of reducing that chain to a single end-to-end entanglement link, and purification operations collapse cyclic subgraphs. These graph reductions can then be implemented via simple substitution rules applied to subgraphs with the respective topology, as per Fig. 8 and Alg. 1.

In this section we discuss some of these observations and how they may be applied.

A. Purification trees

The purification of an arbitrary number of Bell pairs can be described in terms of an operation that maps two Bell states to one. Given states $\hat{\rho}_1$ and $\hat{\rho}_2$, the purified state $\hat{\rho}'$ is,

$$\begin{aligned} \hat{\rho}' &= \hat{\rho}_1 * \hat{\rho}_2 \\ &= \hat{\rho}_2 * \hat{\rho}_1. \end{aligned} \tag{3.1}$$

Given that this operation is non-linear (as seen in Fig. 6), the resultant fidelity may depend on the order in which purifications are applied. Any such ordering can be represented with a binary tree, where states on branches are purified into their intersecting node.

Consider for example the Dür and Deutsch protocols acting on 4 distinct input states $\hat{\rho}_i$,

$$\begin{aligned} \hat{\rho}_{\text{Dür}} &= (\hat{\rho}_1 * \hat{\rho}_2) * (\hat{\rho}_3 * \hat{\rho}_4), \\ \hat{\rho}_{\text{Deutsch}} &= \hat{\rho}_1 * (\hat{\rho}_2 * (\hat{\rho}_3 * \hat{\rho}_4)), \end{aligned} \tag{3.2}$$

where the corresponding binary trees are shown in Fig. 7. Generally, the total number of purification orderings for n states corresponds to the number of n-leaf binary trees,

$$(2n-3)!!. \tag{3.3}$$

Clearly, a naïve search for the optimal purification tree is computationally inefficient. However in Sec. III.B, we demonstrate that for commutative operations (e.g purifications along a common Pauli axis) the resultant purified state is independent of ordering. In the more general case, however, this does not hold and outcomes will be highly order-dependent in general.

B. Entanglement networks as abelian groups

Let us now consider a simple noise model in which only Pauli dephasing channels are applied (i.e there is no noise along other Pauli axes). Then we find that the following algebraic rules hold for our system. Take $F(f_1, f_2)$ to

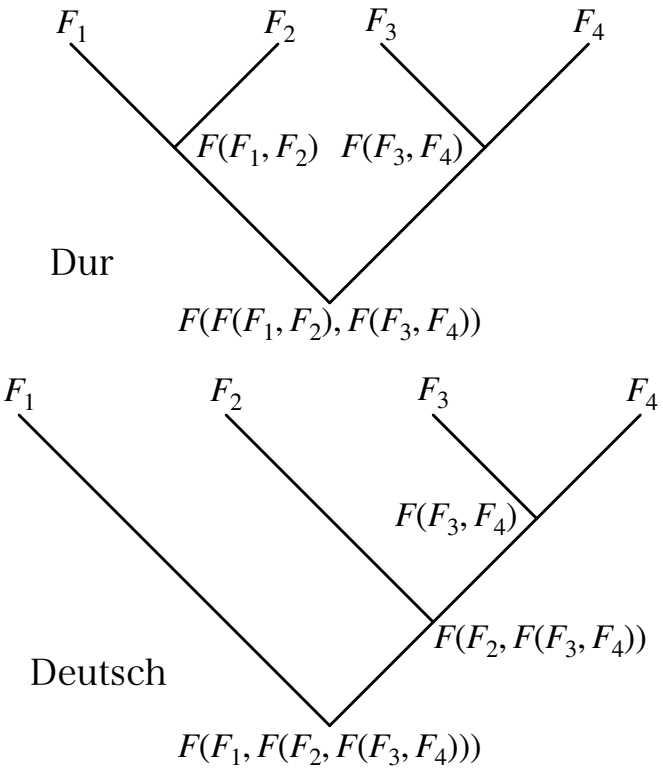

Figure 7: Phylogenetic purification trees for the Dür and Deutsch protocols, representing the ordering in which multiple Bell pairs are purified into a single one. Lines represent noisy Bell pairs, and forks denote purification protocols, where time runs from top to bottom.

be the the fidelity after purification for two states with fidelity f_1, f_2 as given in Eq. 2.17. Then,

$$\begin{aligned} F(f_1, f_2) &= F(f_2, f_1), \\ F(F(f_1, f_2), f_3) &= F(f_1, F(f_2, f_3)), \\ F(f_1, 1/2) &= f_1, \\ F(f_1, 1 - f_1) &= \frac{1}{2}, \end{aligned} \tag{3.4}$$

which in the the domain of $[0, 1]$ allows purification to form an abelian group.

Furthermore, by considering the properties of the entanglement swapping operation S, we find that,

$$\begin{aligned} S(f_1, S(f_2, f_3)) &= S(S(f_1, f_2), f_3), \\ S(f_1, 1) &= f_1, \\ S(f_1, f_2) &= S(f_2, f_1), \\ S\left(f_1, \frac{2f_1 - 4}{2f_1 - 1}\right) &= 1, \end{aligned} \tag{3.5}$$

which is an abelian group under swapping in the domain $[0, 1] \setminus \frac{1}{2}$.

Now, considering success probability, we can define,

$$\begin{aligned} P(p_1, p_2) &= P(p_2, p_1), \\ P(P(p_1, p_2), p_3) &= P(p_1, P(p_2, p_3)), \\ P(p_1, 1) &= p_1, \end{aligned} \tag{3.6}$$

This forms an abelian monoid,

$$\begin{aligned} \hat{\rho}_1 * \hat{\rho}_2 &= \hat{\rho}_2 * \hat{\rho}_1, \\ (\hat{\rho}_1 * \hat{\rho}_2) * \hat{\rho}_3 &= \hat{\rho}_1 * (\hat{\rho}_2 * \hat{\rho}_3). \end{aligned} \tag{3.7}$$

These properties also hold for the success probabilities as well. In the case of purification for a multi-edge graph, there exists a unique reduction, which implies that,

$$\hat{\rho}_{\text{Dür}} = \hat{\rho}_{\text{Deutsch}}. \tag{3.8}$$

This unique reduction is,

$$F = \frac{\prod_{i=1}^{n} F_i}{\prod_{i=1}^{n} F_i + \prod_{i=1}^{n} (1 - F_i)}, \tag{3.9}$$

for the case of fidelity.

It is important to note that for more general error models this relationship no longer holds. The abelian nature of this result ultimately stems from the commutativity of the errors through the underlying processes, which need not hold in general for general error models. For example, in the case of general Pauli channels, the need for twirling prevents the fidelity functions from being associative (Dür *et al.*, 1999).

C. General reduction strategies

More generally, the combined effect of an arbitrary sequence of elementary operations and orderings can be reduced to a single cost-vector. In the instances above we were able to derive these analytically owing to their commutative behaviour and determinism in their ordering. In a more general scenario where operations might not commute and randomisation (e.g via twirling operations) is involved, sampling techniques could be applied to find their average case behaviour and hence equivalent cost-vector.

The greedy multi-path routing algorithm (Alg. 2) is an example of a graph reduction algorithm that reduces a sub-graph to an effective end-to-end cost vector. In the future, we anticipate more sophisticated techniques will be developed based on the application of graph reduction identities, which would be applied on the network in advance to simplify the complexity of subsequent routing algorithms. Alg. 1 shows a computationally efficient algorithm for graph reduction based upon iterative application of such identities. This approach needn't be optimal in general since the outcome is dependent on the ordering of the substitutions, and a full optimisation would involve investigating combinations of these. Despite being

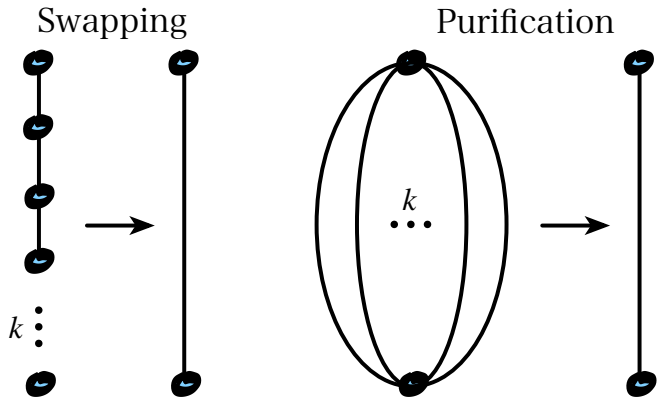

Figure 8: Two graph reduction primitives emerge from our elementary physical devices. Entanglement swapping as a physical primitive, yields reduction rules for mapping linear sub-graphs to a single pair. Entanglement purification allows a 2-cycle sub-graph to similarly reduce to a single pair.

input : graph G, threshold ϵ.
output : reduced graph H.

begin
  $H = G$
  repeat
    $H' = H$
    $H =$ `reduce_cycles(`H`)`
    $H =$ `reduce_linear(`H`)`
    for $e \in E$ **do**
      if $d(e) > \epsilon$ **then**
        $H = H \setminus e$
  until $H = H'$
  return H

Algorithm 1: Pseudo-code for entanglement distribution network graph reduction.

sub-optimal, applying Alg. 1 prior to subsequent routing algorithms (e.g greedy shortest-path, as per Alg. 2) would allow for better utilisation of the graph regions and therefore better entanglement resources between the end-users.

IV. ENTANGLEMENT ROUTING STRATEGIES

We now discuss entanglement routing strategies, which are the ultimate application in graph reduction, where for some number of arbitrary user-pairs, we wish to collapse the entire network graph down to the effective cost vectors between them. We begin by discussing conventional shortest-path routing, before moving onto multi-path routing, a uniquely quantum routing technique.

A. Shortest-path routing

A graph optimisation algorithm we make heavy use of, due to its inherent efficiency, is Dijkstra's shortest-path algorithm (Dijkstra, 1959). For single source and destination, $A \to B$, this exhibits worst-case runtime,

$$O(|V|^2), \tag{4.1}$$

for $|V|$ vertices, which can be reduced to,

$$O(|E| + |V| \log |V|), \tag{4.2}$$

for sparse graphs (Fredman and Tarjan, 1984).

This generalises to the Vehicle Scheduling Problem for n pairs of sources and destinations,

$$\{A_i \to B_i\},\ i = 1 \dots n, \tag{4.3}$$

that must be simultaneously minimised. Unlike Dijkstra's algorithm, this problem does not scale efficiently with n, and is known to be NP-hard in general. Thus, as a greedy approximation heuristic, multiple applications of single-user Dijkstra may be employed instead of performing the full multi-user optimisation.

B. Multi-path routing

Ordinary routing problems involve finding the shortest paths between end-users of a network. With quantum networks however, we are more interested in finding optimal path-sets between end-users. This is because paths in the quantum network represent entanglement links, and with purification, we can make use of multiple paths simultaneously to generate high-quality entangled states. This more general objective of finding the best sets of paths is known as *multi-path routing* (Proctor *et al.*, 2018; Sidhu and Kok, 2020), and its goal is to make use of as much of the network as possible.

This motivates the development of analytic laws that characterise how different network areas relate to the costs associated with routing and purifying entangled states across said areas.

C. Analytic area laws

Consider the case where we have a strand of vertices of depth d where between each pair of vertices there are b edges, defining a region of the graph as per Fig. 9.

Then the log-fidelity between two vertices is given by,

$$\log(F) = \log\left(\frac{2\prod_{i=1}^{b} F_i}{\prod_{i=1}^{b} F_i + \prod_{i=1}^{b}(1-F_i)} - 1\right). \tag{4.4}$$

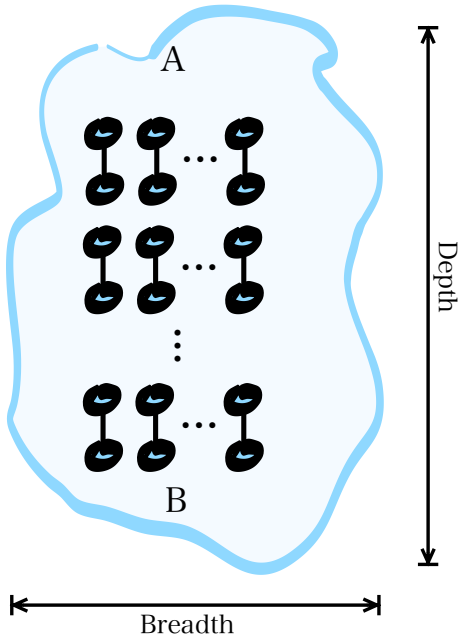

Figure 9: A graph with a regular structure (such as a lattice), or with certain statistical properties (such as random or percolation graphs), will exhibit area laws, relating their geometry to quality of a final Bell-pair that can be prepared across it.

For depth d, the log-fidelity then becomes,

$$\log(F) = \sum_{n=0}^{\infty}(-1)^n \log\left(\prod_{i=1}^{b} F_i - \prod_{i=1}^{b}(1-F_i)\right)^{d-n} \cdot \log\left(\prod_{i=1}^{b} F_i + \prod_{i=1}^{b}(1-F_i)\right)^{n}. \tag{4.5}$$

It is clear that the fidelity of the established entanglement link scales with depth and width as $O(b^d)$. In the case of success probability we can establish a corresponding result. The probability of success for swapping down a chain of length d is ${P_s}^d$ where P_s is the swapper success probability. Then the overall success rate scales as,

$$P_{\text{tot}} = P^{bd}, \tag{4.6}$$

for breadth b. Thus, the failure rate grows exponentially in the area of the circuit.

D. Greedy multi-path routing

Since determining optimal graph regions to allocate to users is in general computationally hard, we define an algorithm based on multiple applications of Dijkstra, which although not optimal in general, provides a highly efficient approximation, whose complexity scales only linearly with the number of users, described in Alg. 2.

input : graph G, source A, destination B, threshold ϵ.
output : Bell pair $\hat{\rho}_{A,B}$.

begin
  pairs $= \emptyset$
  repeat
    $g =$ `shortest_path`$(G_{A\to B})$
    if $d(g) \leq \epsilon$ **then**
      $\hat{\rho}' =$ `reduce`(g)
      pairs $=$ pairs $\cup\, \hat{\rho}'$
      $G = G \setminus g$
  until $d(g) > \epsilon$
  $\hat{\rho}_{A,B} =$ `purify`$(pairs)$
  return $\hat{\rho}_{A,B}$

Algorithm 2: Pseudo-code for the greedy shortest-path-removal algorithm for multi-path entanglement routing.

Conceptually, this algorithm iteratively eliminates shortest paths between end-points up to a cutoff threshold. These paths all parse into a purification protocol to reduce the traversed region into a single entanglement link.

This is trivially generalised to the multi-user context with an additional inner loop over the end-user pairs, providing a computational overhead only linear in the number of users. An example application of the greedy multi-user, multi-path routing algorithm to a lattice network is shown in Fig. 10.

E. Multi-user routing

Given that multi-path routing reduces a sub-graph of G to an entanglement link between end-users, the multi-user case is equivalent to a graph partitioning problem.

Let us assign G_i to each pair of users $A_i \to B_i$. These sub-graphs partition the entire graph, such that,

$$G = \bigcup_i G_i,$$
$$G_i \cap G_j = \emptyset \ (i \neq j), \tag{4.7}$$

illustrated in Fig. 11. This yields an algorithmic generalisation of Alg. 2 to the multi-user case, provided in Alg. 3.

V. THE PHILOSOPHY OF QUANTUM VS. CLASSICAL NETWORKING

From our theoretical framework, there emerge a number of distinct conceptual and philosophical principles that distinguish multi-path entanglement routing networks from conventional digital networks:

- In classical networks we conceptually desire to use the *shortest available path* within a graph to form a

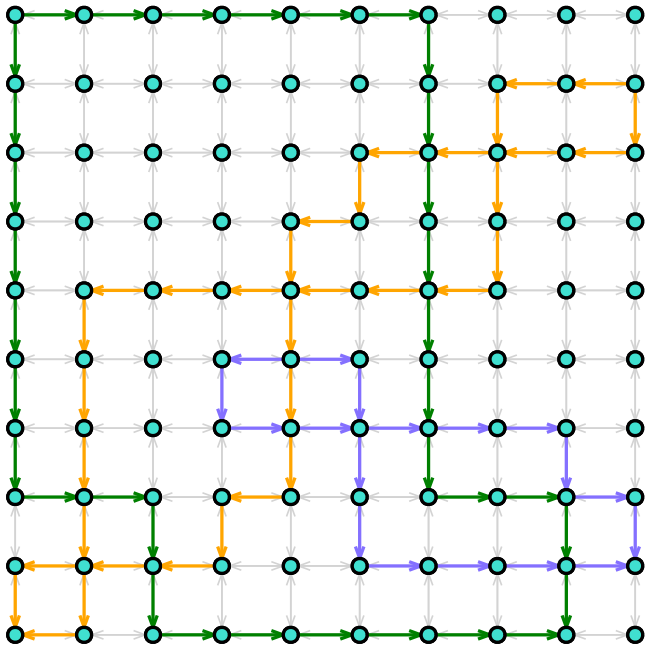

Figure 10: Example execution of the greedy multi-user, multi-path routing algorithm for 3 user-pairs on a 10×10 lattice. Colour coding denotes which channels are allocated to which user-pairs by the algorithm. For each user-pair, resultant paths are finally purified together, yielding end-to-end entanglement links of higher fidelity than the individual shortest-paths. Fig. 19 provides a similar example for multi-user temporal routing.

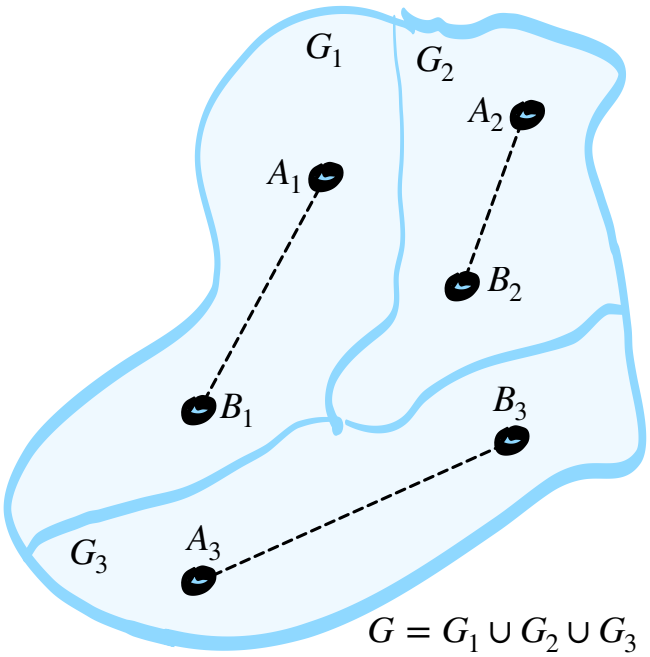

Figure 11: For multi-user networks, we associate a sub-graph G_i to each pair of users $A_i \to B_i$. These sub-graphs partition the entire graph, and a metric is associated with each sub-graph, specifying its quality (e.g effective fidelity). A graph-partitioning algorithm is to employed to find an optimal (or approximation thereof) partitioning that satisfies constraints imposed on the metric associated with each sub-graph. Shown above is an example for a 3-user network.

input : graph G, sources $\vec{A}$, destinations $\vec{B}$, threshold ϵ.
output : Bell pairs $\{\hat{\rho}_{\vec{A},\vec{B}}\}$.

begin
  pairs $= \emptyset$
  repeat
    $\vec{g} =$ `multi_user_shortest_path`$(G_{\vec{A}\to\vec{B}})$
    if $d(g_i) \leq \epsilon \, \forall \, i$ **then**
      $\hat{\rho}' =$ `reduce`$(\vec{g})$
      pairs $=$ pairs $\cup \, \hat{\rho}'$
      $G = G \setminus \vec{g}$
  until $d(g_i) > \epsilon \, \forall \, i$
  $\hat{\rho}_{\vec{A},\vec{B}} =$ `purify`(pairs)
  return $\hat{\rho}_{\vec{A},\vec{B}}$

Algorithm 3: Pseudo-code for the multi-user implementation of the iterative shortest-path removal algorithm for multi-path entanglement routing. Note that this relies on a multi-user shortest-path subroutine, which are NP-hard in general. However efficient approximations such via sucessive applications of Dijkstra could be employed instead.

communication link (e.g using a Dijkstra-type shortest path algorithm) whereas in the quantum case we desire to exploit the *optimal subgraph* between two points — the subgraph that upon reduction provides the optimal best possible end-to-end cost vector.

- Equivalently, in the classical case we wish to minimise use of the network graph, whereas in the quantum case we want to exploit all of it.

- In the multi-user scenario, both multi-user shortest-path algorithms (in the classical case), and optimal graph partitioning algorithms (in the quantum case), are NP-hard in general to perform optimally. However, heuristic approximation methods for these have been well studied (and obviously our current classical internet relies heavily on such sub-optimal approximation techniques).

- Multi-path entanglement routing can be considered conceptually similar to the classical notion of *load balancing*, whereby instead of maximising bandwidth by distributing data-packets via redundant routes, we are engaging in *decoherence balancing* by distributing entanglement via redundant routes and subsequently purifying them into one.

- Because entanglement purification consumes Bell pairs in order to increase fidelity, it induces a direct trade-off between bandwidth (i.e the rate of Bell-pair distribution) and fidelity, since it necessarily consumes Bell-pairs in the process.
- Much like classical resistance networks, adding resources to a quantum network cannot decrease network performance. Redundant pathways in quantum networks are in fact highly desirable since they imply additional possibilities for graph reduction/routing.

VI. QUNET: A PACKAGE FOR SIMULATING QUANTUM NETWORKS

`QuNet` is open-source software for simulating entanglement networks and benchmarking entanglement routing algorithms, available at https://peterrohde.github.io/QuNet, including source code, documentation, and the demonstration files used to generate the results presented here.

A. Related work and motivation

Several quantum internet simulators currently exist, the most established of which are (in no particular order) `NetSquid` (https://www.netsquid.org) (Coopmans *et al.*, 2020), `QuNetSim` (DiAdamo *et al.*, 2020), `SQUANCH` (Bartlett, 2018), `QuISP` (Matsuo, 2019) and `SimulaQron` (Dahlberg and Wehner, 2018). Although these packages differ in their methodology, they share the following similarities to some degree:

- Network agents (end-users) hold registers of qubits.
- There exists a scheme for relating the local registers in such a way to describe entangled states that are shared between end-users.
- The evolution of the underlying quantum states of the network is simulated under some combination of local operations and measurements, usually by interfacing the software with an existing quantum circuit simulator.
- Noise effects, which are often time sensitive, and or event broadcasting are implemented with the use of a discrete-time event engine.
- The goal is to test end-user applications, the scope of which is predominantly low-level communication protocols, or towards the development of a quantum protocol stack.

The primary distinction of `QuNet` is that it considers a subset of error channels that are expressible in terms of additive cost metrics. This allows us to represent complex quantum networks with a simple set of weighted graphs (one graph for each cost). `QuNet` therefore operates at a high level of abstraction as opposed to a low-level link layer where the control sequences of individual network components are implemented.

In using this approach we are able to exploit existing graph theoretic routing algorithms, which are computationally efficient and well-studied. Furthermore, we are able to extend these techniques to accommodate for quantum memories using temporal meta-graphs, described in Sec. VI.C. A limitation of this approach is that it doesn't lend itself to modeling arbitrary channels, in particular non-commutative ones that cannot be expressed as additive metrics.

B. Design principles

The goal of `QuNet` is to perform *cost-vector analysis* in quantum networks, based on user demand, to make optimal routing decisions. Because `QuNet` is highly algorithmically efficient, it could be employed for overseeing quantum networks and making real-time routing decisions for the purposes of classical control of the network in the response to live user demand. `QuNet` employs the following methodology:

1. Given a graph with a number of end users, we apply sequences of elementary physical operations (notably purification and swapping) to perform graph reduction, yielding equivalent cost vectors for established entanglement links.
2. Efficient cost vector analysis algorithms are performed on the graph to find optimal routing strategies for establishing these entanglement links in response to end-user requests.

The principle advantage of `QuNet`'s cost vector approach is that it does not require direct tracking of quantum states, thereby bypassing some quantum complexity issues, and ensuring compatibility with existing graph theoretic techniques.

`QuNet` is based on the following design considerations, and structured as shown in Fig. 12:

1. `QuNet` is written in Julia (https://www.julialang.org), a high level language that compiles to high-performance native code, interfaces with Python and C/C++, and can be embedded into interactive Jupyter (https://www.jupyter.org) notebooks.
2. We ensure scalability for large networks by utilising only computationally efficient routines and avoiding complex combinatoric optimisation. Most notably, we rely heavily on Dijkstra's shortest path algorithm, which is highly efficient in graph size.

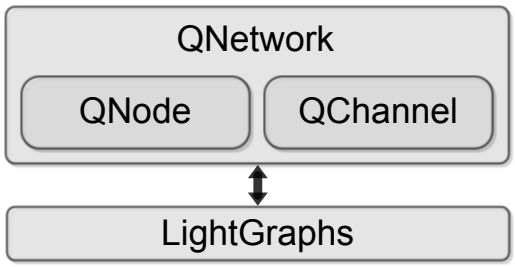

Figure 12: Users interact with the `QuNet` package via `QNetwork` objects, comprising any number of `QNode` and `QChannel` objects. `QuNet` interfaces with the `LightGraphs` package to implement core functionality, which is interchangeable for other graph libraries, and which users do not interact with directly.

3. Graph library independence: although the current implementation relies on the Julia `LightGraphs` package (`https://www.juliagraphs.org`), this is designed to be easily interchangeable for any graph library implementing the necessary primitives. A current limitation is that `LightGraphs` does not provide support for multi-graphs.

4. Users interface with `QuNet` using only a `QNetwork` object and its constituent `QNode` and `QChannel` objects, which are graph library agnostic.

5. Dynamic simulations: nodes may not be stationary, as is the case for satellite nodes, in which case the cost vectors of associated channels dynamically update accordingly. `QuNet` accommodates for different channel types, including free-space and optical fibre links, with their respective decay characteristics.

6. Network abstraction: `QuNet`'s `QNode` and `QChannel` types can take arbitrary form, independent of the underlying technological implementation. Cost vectors needn't be restricted to representing device-level properties, but could abstractly represent entire device sequences by reducing them to their equivalent cost vector. For example, an entire quantum repeater sequence (Gisin and Thew, 2007; Munro *et al.*, 2008, 2015; Sangouard *et al.*, 2011, 2007) comprising complex control over swapping and purification operations could be reduced to a single abstract `QChannel` representing its net effective cost vector. Similarly a large SneakerNet (Devitt *et al.*, 2016) channel, in which entanglement is physically transported under heavy error correction, can be represented by a single `QChannel` representative of overall state decay under that mode of communication, independent of its internal operation. Thus, a `QNetwork` object can represent an entire network at any level of abstraction, ranging down from the device level up to high level abstractions of constituent sub-networks, backbones, or regions of interest.

C. Simulating quantum memories with temporal meta-graphs

A major problem facing multi-user networks is congestion as the number of competing users increases. Obviously, the availability of quantum memories (Gouët and Moiseev, 2012; Lvovsky *et al.*, 2009) can easily overcome congestion by enabling qubits to wait until channels become available for their use. Many conventional multi-user graph optimisation techniques are highly inefficient as the number of users increases, since combinatoric optimisation must be employed. To overcome this, we developed a temporal optimisation algorithm based on Dijkstra's algorithm that is highly efficient and bypasses any combinatoric optimisation.

The algorithm and its computational complexity are described in detail in App. A. The concept of the algorithm, based on so-called *temporal meta-graphs* is shown in Fig. 13.

The overall computational complexity of multi-user route-finding using temporal meta-graphs scales as,

$$O(M^3V^2), \tag{6.1}$$

where there are M user-pairs in a V-node graph.

A natural expectation is that temporal links are all fixed in the same direction. Surprisingly however, temporal links could be bidirectional for system comprised of alternating entanglement sources and swapper nodes. This is shown in Fig. 14. The reason for this bidirectionality is that entanglement swapping is not a time sensitive operation. A sequence of swaps needn't be performed in a specific chronological order.

In a similar but unrelated vein, asynchronous links can be manipulated for different timing requirements. For example, if Alice strictly requires that she receive her qubit at a given time(s), then every one of her incoming asynchronous edges that do not satisfy her time condition can be removed. Similarly, if Bob wishes to send a qubit at a given time(s), then all his outgoing asynchronous edges that fail his condition can be removed. The asynchronous edges chosen by a temporal routing algorithm specifies a routing queue for users.

VII. ADVANCED ROUTE OPTIMISATION IN ENTANGLEMENT DISTRIBUTION NETWORKS USING QUNET

We now showcase the capabilities of `QuNet` by benchmarking our greedy multi-path routing algorithm against a range of relevant network scenarios. To aid in benchmarking, we limit ourselves to the study of square lattice networks, however `QuNet` is equally readily applicable to arbitrary network topologies and routing strategies. Here, we use `QuNet` to investigate network performance the following scenarios:

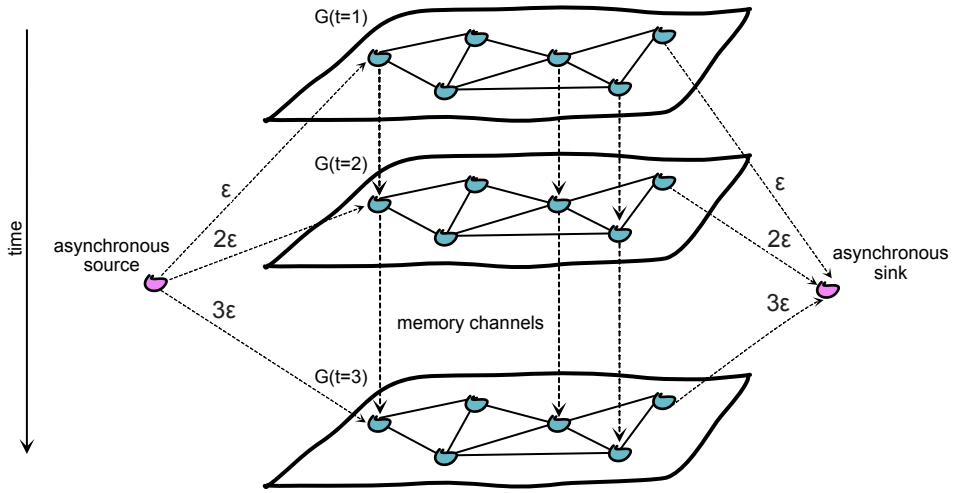

Figure 13: A temporal meta-graph is constructed by layering instances of the underlying graph over some number of time-steps, T. Nodes possessing quantum memories have vertical directed edges connecting the node to itself at the next time-step, representing a delay. To find a route from A to B, we construct dummy *asynchronous nodes* for each. The asynchronous source for A connects outwardly to all nodes A for each time-step. Similarly, the asynchronous sink for B connects inwardly to all nodes B for each time-step. Thus, the asynchronous nodes allow the route-finding algorithm to discover all nodes associated with A and B throughout the entire temporal meta-graph. The incremental weights ϵ guide route-finding to prioritise the earliest available time-slots for a given user. Thus by increasing the overall graph by a factor of T, we remain fully compatible with existing route-finding algorithms based on shortest-path removal, and retain their associated efficiency, without the need for any temporal combinatorics. Fig. 19 shows an actual example from a `QuNet` simulation, demonstrating channel allocation to multiple user-pairs under multi-path temporal routing.

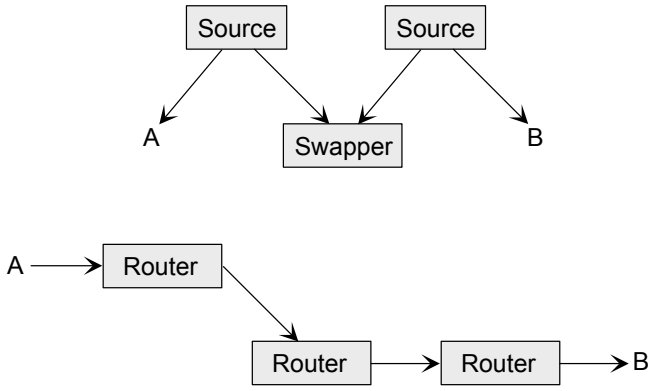

Figure 14: Two examples of entanglement routing between users A and B, where time flows downwards. (top) An alternating sequence of entanglement sources and swappers. Here the path between A and B is allowed to route backwards in time since entanglement swapping is time-independent. (bottom) A simple sequence of qubit routers, which cannot route backwards in time.

- Single-user networks with purification-based multi-path routing.
- Multi-user networks in the context of competition and congestion effects.
- Percolated networks with random channel failure.
- Overcoming multi-user network congestion through network scaling.
- Overcoming multi-user network congestion via temporal routing and the use of quantum memories.

Our greedy multi-path algorithm represents the simplest such algorithm that is suited to cost-vector analysis, but is readily adaptable and allows many opportunities for further optimisation for quantum network engineers.

A. Benchmarking multi-path purification with single-user networks

The primary goal of `QuNet` is to use efficient, classical cost-vector analysis to predict the expected performance of a quantum network, thus avoiding the need for full quantum-state simulations of a complex network. Entanglement swapping and multi-path purification are the critical elements that allow quantum network links to be established in the presence of real-world imperfections like loss and decoherence. To validate and benchmark `QuNet`'s performance in simulating these elements, we first study the simplest possible case for multi-path routing of a single, randomly chosen user pair in a rectangular lattice, and in particular how this performance varies with network size.

For this context, we consider a rectangular lattice of variable size n, where each link is affected by both loss and dephasing noise with a 1dB cost to the loss rate and the dephasing probability respectively. For each trial, we select a random user pair in the network, and use

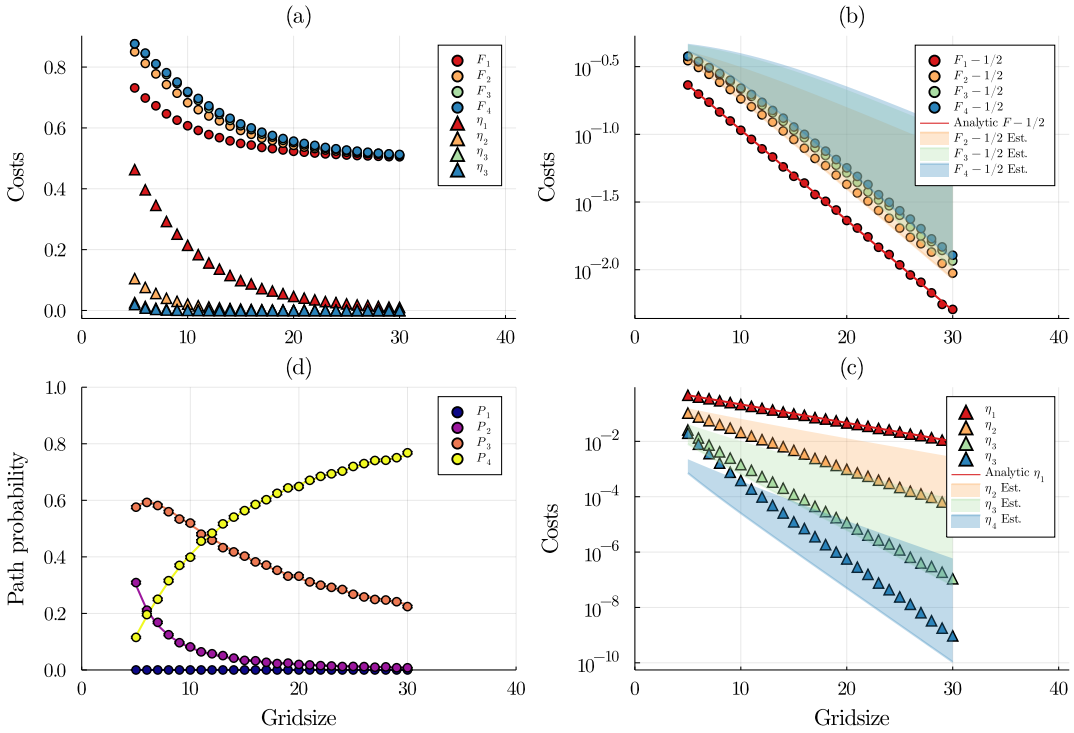

Figure 15: Single-user network performance versus grid size for different numbers of maximum allowed (edge-disjoint) paths. For each trial run, one random user pair was selected on a $n \times n$ rectangular lattice and was routed using `greedy_multi_path`. Each edge has 1dB costs in efficiency and fidelity, and each data point is the average of 5000 random trials. **(a)** Average routing costs in terms of efficiencies η_j and fidelities F_j, where j is the maximum number of allowed paths. **(b, c)** Average costs plotted on a log scale for fidelity $(F_j - \frac{1}{2})$ (b) and efficiency (c). A solid line is plotted for the one-path case where an exact analytical solution is known. For the multi-path cases, the shaded areas show estimated expected scalings for each case, based on analytical approximations. **(d)** Probability P_j that a user finds j paths in the case where up to four paths may be purified. Analytical curves for each path probability are overlaid.

our `greedy_multi_path` algorithm to identify a good set of paths connecting the two users, up to some specified maximum number of allowed paths. This allows us to explicitly study the effect of multi-path purification on single-user network performance. In this context, where there is no competition between user pairs, the number of available paths will then be further constrained only by the degree or connectivity of each end user, which is determined by their location near the edge or within the body of the graph.

We present the results for this scenario in Fig. 15. The average fidelity and efficiency of a transmitted Bell pair is given in Fig. 15(a). As expected from the post-selective nature of the purification process, we see fidelity increase with successive purifications at the cost of decreasing efficiency. We also find that both the fidelity and efficiency decrease with grid size, due to the consequent increase in average distance between randomly selected user pairs. For a rectangular lattice, the average separation between two vertices, known as the average L1 or Manhattan distance, scales linearly with the grid size according to the fraction $\frac{2}{3}n$ (See App. B). By plotting the fidelity and efficiency costs on a log scale (Figs. 15(b,c)), except at small n, we confirm that these costs scale exponentially towards their asymptotic values of $\frac{1}{2}$ and 0, respectively, as expected from Eq. 2.6. We see some deviation from this asymptotic scaling at small grid sizes, which we attribute primarily to edge effects that arise because end users located at the edge may not have access to the maximum number of paths available for purification. These edge effects, and the fact that they diminish with grid size, are illustrated in Fig. 15(d), which shows the probabilities that a randomly chosen user pair will have access to a certain number of paths as a function of the grid size.

Having validated `QuNet`'s qualitative predictions, we now turn to the question of how to validate its quantitative performance against analytical expectations. In fact, predicting the behaviour of complex networks analytically in any scenario involving competition is a very challenging problem. This is a scenario that arises naturally in the case of quantum networks where the aim is to exploit multi-path routing for the purpose of purification. For a single path, Fig. 15 shows that `QuNet` agrees exactly with a simple analytical prediction calculated as a function of average Manhattan distance. As soon as purification is incorporated, however, even for simple single-user network-

ing scenarios, the path competition that this introduces increases the difficulty of the analytics combinatorically. This is exactly why a numerical simulation package like `QuNet` is invaluable for benchmarking quantum networks.

Here, we identify three effects that complicate the calculation of analytic costs in the context of networks with purification. Firstly, the lengths of available network paths will depend on whether the end users lie in the same row or column. To illustrate, let L be the Manhattan distance between an end-user pair in the middle of a large grid lattice (that is, neither end user located on a lattice edge). The four shortest edge-disjoint paths connecting them will have lengths $(L, L+2, L+2, L+8)$ for users in the same row or column, and $(L, L, L+4, L+4)$ otherwise. The proportion of user pairs in each category is easily calculated, at least in the single-user case: The chances of selecting a user pair in the same row or column diminishes quadratically with grid size, and this fraction can be neglected if the grid is sufficiently large. Secondly, users on the boundary of the network have constrained connectivity, and therefore may not be able to utilise up to the maximum number of allowed paths for purification. Again, the proportion of user pairs affected by this is readily calculated: Fig. 15(d) shows first that an analytical calculation of available path probabilities (solid lines) exactly agrees with the numerical data obtained from `QuNet` simulations, and second that this effect also diminishes with grid size, and can be neglected for large enough grid sizes. Except for the next effect, both of these could be readily accounted for in analytical calculations, but the final issue, that arises because purification leads to non-linear propagation of costs (Eq. 2.17), is unavoidable. For example, the average costs associated with purified paths (averaged over randomly selected user pairs) is not equal to the cost of purified paths calculated from the average Manhattan distance between user pairs, which is how we predicted the single-path costs in Fig. 15. Unfortunately, calculating the proportion of users separated by a given Manhattan distance when randomly selecting both users in a pair on a fixed finite grid increases in difficulty combinatorically, compounded by the first two effects described above. This is already prohibitively difficult for the single user pair case, and only becomes more challenging for more complicated scenarios involving complex network topologies or competition between multiple user pairs. As a result, using a package like `QuNet` which enables a Monte-Carlo random-sampling approach becomes a much simpler and more efficient way to calculate costs in the context of purification.

Because of this, we elected to check our multi-path data against two oversimplified estimates that do not account for the non-linearity of purification, but provide a rough region for the expected values, and help establish confidence that `QuNet`'s purification scheme is working correctly. These estimates, which define the edges of the shaded regions in Figs. 15(b, c), are calculated by purifying a set of paths with lengths given by the edge-disjoint path sets described above—$(L, L+2, L+2, L+8)$ for users in the same row or column, and $(L, L, L+4, L+4)$ otherwise—with L taken to be the average Manhattan distance for a given lattice size.

B. Multi-user, multi-path routing

Competition between end-users is an important consideration in any network, but is especially significant in quantum networks, where information to be shared cannot be cloned to mitigate against the inevitable effects of transmission loss, and purification is instead required. As such, understanding how user demand and competition affects overall network performance is extremely useful in the design of quantum networks. Here, we benchmark the performance of our `greedy_multi_path` algorithm for a 10×10 grid lattice with an increasing number of randomly selected user-pairs up to the fully saturated limit of 50 user pairs. Each link has a 1dB cost in loss rate and dephasing probability, and users can route up to the maximum four edge-disjoint paths allowed by the degree of graph connectivity. The results of this scenario are shown in Fig. 16.

Fig. 16 (top) shows how average networking costs change with the number of competing user pairs. As discussed in Sec. II.B.4, we analyse the network performance in terms of complementary costs, efficiency and conditional fidelity. Starting from the maximal fidelity expected for the 10×10, single-pair case already analysed in Fig. 15, we see the fidelity initially decrease, before flattening out to a steady-state value after approximately 10 user pairs. By contrast, while the efficiency initially increases, it reaches a maximum value at around 10 user pairs, before decaying away towards zero. The initial change reflects the fact that as more users are introduced into the network, fewer user pairs are able to access multi-path routing, and without the ability to exploit the post-selective purification process, this leads to higher efficiencies, but lower fidelities. In Fig. 16 (bottom), we see that the rates associated with users finding multiple paths all decrease rapidly, and the proportion of users finding only one path increases to a maximum at around 10 user pairs. However, we also see a new effect, arising due to multiuser competition, namely that the proportion of users finding no paths (P_0) increases rapidly after the same point. Thus while the conditional fidelity appears to reach a steady-state value even for large numbers of users, the decaying overall efficiency for a randomly selected user pair highlights that the network becomes less and less effective at distributing entanglement. To isolate the different efficiency effects at play, we also plot a conditional efficiency cost, where the efficiency is averaged only over those users who are able to find at least one path. Now, the efficiency also reaches a steady state value

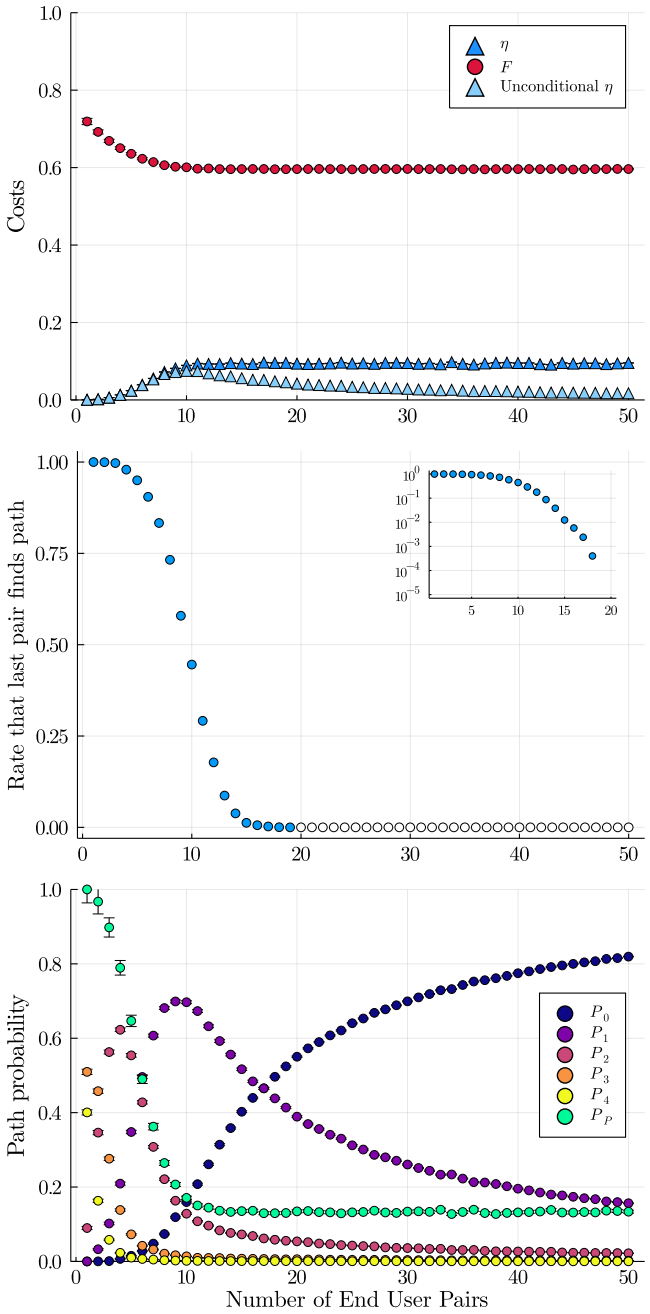

Figure 16: Network performance with the number of competing end users. For each sample, n random userpairs were selected on a 10×10 grid lattice and were routed using `greedy_multi_path`. Each edge has 1dB costs in efficiency and fidelity, and each data point was collected with 5000 samples. (top) Average routing costs in terms of average conditional efficiency η, average conditional fidelity F, and average unconditional efficiency. (middle) The probability that the last userpair queued in `greedy_multi_path` finds at least one path. Unfilled circles are data points where no path was found in the 5000 samples. [top right] log plot. (bottom) Probability P_j that a user finds j paths. P_P is the probability of purification, that is, the likelihood a userpair finds at least two paths between them.

after around 10 user pairs. In this multiuser scenario, `QuNet`'s greedy multipath algorithm cycles sequentially through all randomly chosen user pairs (in a fixed order), looking first for one path each, then more paths. Fig. 16 (middle) shows that the rate at which the final user finds at least one path decays very rapidly towards zero, and shows that even though it is possible to choose up to 50 non-colocated user pairs in a 10×10, overall network congestion increases very rapidly and the network capacity effectively reaches full saturation at many fewer user pairs. And once new user pairs can no longer find any new paths, adding users no longer affects how many paths can be found by the other user pairs and the distribution over path numbers remains constant. Indeed, by aggregating the multiple-path rates into a single probability of a user pair being able to access purification, P_P, we see that this probability drops rapidly and monotonically from 1 to a low steady-state value at around 10 user pairs, with the curve closely tracking the shape of the efficiency curve observed in the top panel. These results are consistent with the change in purification rate being the main effect driving the changing path costs in this multiuser setting.

C. Channel percolation effects

Real-world networks inevitably fail when nodes or channels malfunction. This leads to the notion of *percolation theory* in networks (Bollobás and Riordan, 2006; Kesten, 1982; Stauffer and Aharony, 1992), which shows that communication can remain robust provided failure rates lie below some percolation threshold associated with the topology. Although this is something well-understood in classical networks, we start to explore how the dynamics may vary in quantum networks where multi-path routing may be utilised. For this scenario, we consider a single random user pair routed on a 10×10 grid lattice where each edge has an identical probability of being removed. As before, surviving edges have 1dB costs in loss and dephasing. Fig. 17 (top) shows how the routing costs of our algorithm vary with the percolation rate in terms of average fidelity (F) and efficiency (η). At percolation probability equals zero, this scenario reduces to the single-user, multipath routing scenario studied in the previous figures, so the costs start from same, previously calculated values. As the percolation probability increases, however, the cost trends show two distinct regions, which we now explain.

In the first region, at percolation probabilities up to around 0.4, we see that fidelity steadily decreases, while the efficiency increases. (Plotting the log of efficiency, not included here, shows that the efficiency initially increases exponentially with percolation probability.) This behaviour is a result of changing purification rates. From Fig. 17 (bottom), which shows the rates at which the user pair finds multiple paths, we observe a steady trend, as

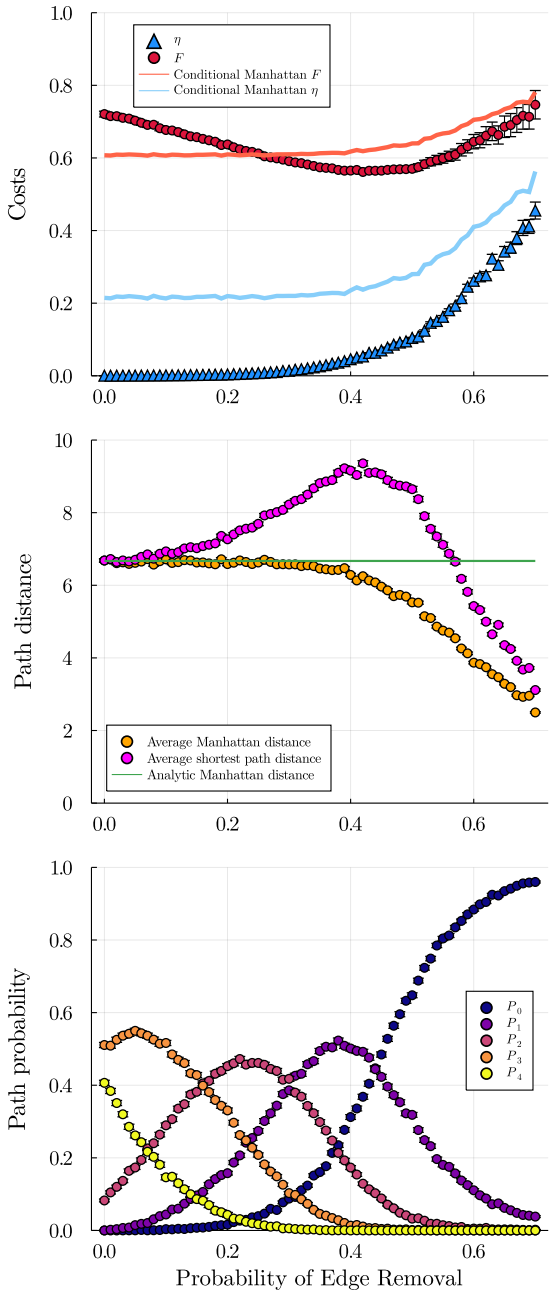

Figure 17: Network performance with edge percolation rate. For each sample, one randomly chosen userpair on a 10×10 grid lattice was routed using `greedy_multi_path`. Each edge has 1dB costs in efficiency and fidelity, and every edge has an identical probability of being removed. Each data point was collected with 5000 samples. (top) Average costs for routing in terms of the efficiency η, and fidelity F of the Bell pair. The solid lines are the average Manhattan distance postselected on whether the userpair is connected in the network. (middle) [left] the average Manhattan distance and the average shortest path distance between the userpair, both of which are post-selected on whether the userpair is connected. (bottom) Probabilities of different path finding scenarios such that P_j is the case that j paths were found between the userpair.

expected, towards fewer paths being available for use in multipath purification. Since purification increases fidelity at the cost of efficiency, this trend results in decreased fidelity and increasing efficiency as a function of percolation probability.

In the second region, the efficiency continues to increase, but the fidelity turns around and starts increasing again. Recall, however, that here we are plotting the conditional fidelity. As with the previous multi-user scenario, increasing percolation rates introduce effective competition into the network, and we see an increasing probability that even a single user pair fails to find any viable communication paths. In the 10×10 lattice case, this starts to be significant for percolation probabilities above approximately 0.3 to 0.4 (Fig. 17 (bottom)).

To understand why this leads to increasing fidelities, we plot two complementary measures of average user pair separation (Fig. 17 (middle)). The average shortest path distance calculates the length of the shortest available path between the user pair. The initially increase in this value highlights the fact that percolation forces users to communicate via more circuitous paths to detour around missing links. Despite this effect, we see that this path length steadily decreases after percolation probabilities of around 0.4. The conditional average Manhattan distance (calculated for sample pairs with available communication paths) shows no similar initial increase, but also steadily decreases for percolations above 0.4. Since this quantity depends only on the users' relative positions, this decrease directly reflects the fact that far separated user pairs become significantly less likely to find any available paths for large percolation probabilities. The graph begins to break up into multiple disconnected patches, and user pairs located on different disjoint patches are unable to find a viable communication path. The conditional Manhattan distance provides a measure of the typical size of intact patches, and the disparity between it and the conditional shortest path distance provides a measure of the irregularity of shape in these patches. Because only closer spaced user pairs survive, both fidelity and efficiency costs increase for higher percolation rates. We can also illustrate the changing conditional Manhattan distance directly in the corresponding expected costs (Fig. 17 (top)). When the percolation probability is small, the ability to purify multiple paths on average causes a strong mismatch between these costs. For large percolation rates, however, where purification capacity is limited, the simulated costs converge towards the values predicted from the conditional average Manhattan distance.

D. Network scaling effects

In the previous sections, we demonstrated two competition effects, user congestion and link percolation, which hinder the performance of multi-path entanglement rout-

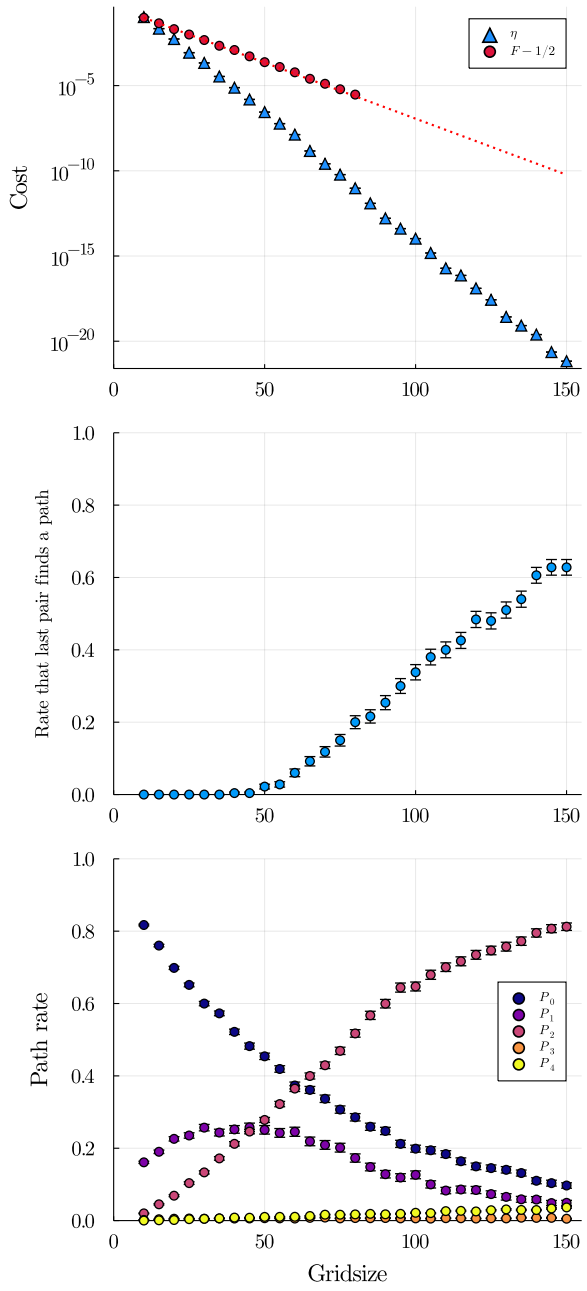

Figure 18: Routing data for fifty randomly chosen userpairs using using `greedy_multi_path` on a grid lattice with variable size. Each edge has 1dB costs in loss and dephasing probability, and each data point was collected with 500 samples. (top) Average multipath routing costs, shown in log scale, for the efficiency η, and fidelity F of the Bell pair (or rather, $F - \frac{1}{2}$). Note that, in log scale, the fidelity data does not show across the full range, because the fidelity rapidly saturates to its asymptotic value of 0.5 beyond the floating point precision used to store the data. (middle) Probability that the last pair is able to find at least one path between them. (bottom) Probabilities of different path finding scenarios such that P_j is the case that j paths were found between the user pair.

ing. Here, we consider strategies to ameliorate the effects of competition, which we will demonstrate for the case of network congestion. A simple, if perhaps brute-force strategy for mitigating competition is to increase the scale of the network.

To explore this scenario, shown in Fig. 18, we start with the same fully saturated 10×10 rectangular lattice network with fifty randomly chosen end-users that was studied in Fig. 16, and analyse performance as we increase the size of the network. As before, each edge has a 1dB cost in loss and dephasing probability. In this scenario, we expect that as we decrease the relative density of user pairs, more links will be routed on average in exchange for a larger average path length. Fig. 18 (top) is a logarithmic plot showing the average routing costs in terms of η and $F - \frac{1}{2}$ versus grid size, the clear linear trends showing the expected exponentially decaying success probabilities with average path length. What is perhaps somewhat surprising is that this effect completely dominates any improvement in congestion that might have been expected to result from increasing the number of paths available for path routing.

As seen in Fig. 18 (bottom), and earlier, for the fully saturated 10×10 lattice, there is more than an 80% chance that a randomly chosen user pair will not be able to find any viable communication pathways. In Fig. 18 (bottom), we also see that the proportion of users that do find paths increases rather rapidly with gridsize. Despite this, Fig. 18 (middle) shows that the rate that the last (50th) user is able to find a path does not start to increase significantly until we reach a grid size around 50×50 (a network 25 times larger than the initial 10×10 case). Even then, this increases rather slowly, not even exceeding 50% until a lattice size around 130×130, by which point the end-user pairs already occupy just a fraction of a percent of the total nodes. The proportion of users finding the most paths (3 or 4) increases even more slowly. Indeed, across the full range, P_3 and P_4 combined only reach around 5%, whereas P_2 (still increasing) reaches in excess of 80%, substantially larger than the maximum P_2 reached in either Fig. 16 or 17.

By comparison, the probability a random user pair will have the connectivity required to find 3 or 4 paths in principle, is already much larger than 99%. These results indicate that it is much more difficult to unlock paths by expanding the size of a network than it is to increase congestion by adding user pairs. Furthermore, the exponential increase in path costs associated with a larger network, more than counterbalances any potential improvement in multipath routing that the larger network enables. Even when the user-pairs make up a tiny fraction of the total number of nodes, we still find significant competitive effects that limit the multi-path routing capacity. Increasing lattice size is therefore clearly an ineffective strategy for solving network congestion in multipath entanglement networks. In the next section, we explore the alternative paradigm for mitigating con-

gestion with temporal multiplexing, rather than spatial multiplexing.

VIII. TEMPORAL MULTIPLEXING IN ENTANGLEMENT DISTRIBUTION NETWORKS USING QUNET

A. Network Performance with Time-depth

In this section, we use our temporal meta-graph formalism developed in Sec. VI.C to study the performance of a temporal multiplexing strategy. For consistency, we again start with a fully saturated 10×10 rectangular lattice with 50 user-pairs and, this time, analyse the routing performance as we increase the temporal depth. A simplified example of this temporal multi-path routing is illustrated in Fig. 19.

In this simulation scenario, we equip each node with one bit of lossless quantum memory for multi-path routing, which allows our `greedy-multi-path` algorithm to find paths that route between temporal-layers. Here, we are interested in the simplest possible routing scenario where there are no temporal routing constraints, so that any path connecting a user-pair should be valid, irrespective of whether the ends of the path lie on the same temporal layer. Our first assumption, however, that each node has a lossless memory, does not guarantee that this unconstrained routing will always be possible. To this end, we therefore endow each node with an auxiliary bit of lossless quantum memory, to facilitate multipath purification by allowing users to store an intermediate state until the next qubit is routed to the end user. One memory is always sufficient for such routing, since multiple Bell pairs can be purified sequentially, such that at most one bit needs to be stored at a given time step. In addition, we impose a four-path limit for each pair so that our comparison is consistent with that of the previous section.

We present the results of this new simulation in Fig. 20. Fig. 20 (top) has the average routing costs of the network versus the maximum temporal depth of the meta-graph. The two dotted lines show the asymptotic "competition-free" values for average efficiency η and fidelity F, respectively, calculated by considering the single-user case with up to five temporal layers available for redundancy. Fig. 20 (bottom) shows the average path probabilities for a given user in the network. Here, we find that only a few temporal slices are required to completely resolve the effects of multi-user competition. In Fig. 20 (bottom), we see P_0 rapidly becomes negligibly small: Only five time steps are needed for the congestion effects in a fully saturated, 50 user-pair network to be completely mitigated. This is consistent with our previous observations from Fig. 16 that the performance of a 10×10 network saturates at around 10 user-pairs, because of the large end-to-end path failure P_0.

Increasing the temporal depth further, we see network performance quickly improves towards its optimal costs. Indeed, when using just fewer than 15 layers, we see our network is comparable in performance to an identical network with just a single user-pair. Far fewer effective nodes are required to achieve such performance than for spatial multiplexing. We also note how the path probabilities of Fig. 20 (bottom) strongly contrast those of Fig. 18, where even the largest graphs have only a marginal increase in multi-path capacity. Here, on the other hand, the time-depth capacity is maximised after just fifteen temporal layers.

Another key benefit of temporal multiplexing is the ability to circumvent edge effects. In Figs 15 and 16, even the single user-pair case, without any competition, does not achieve maximum multi-path capacity, because user pairs located at the boundary of the lattice do not have access to the same number of connecting links, and these edge effects only vanish for very large grid sizes. In a temporal multiplexing scheme, however, the number of paths that can be routed does not only depend on the connectivity of the node, but is augmented by the maximum time-depth. Thus, for applications where very high fidelity states, and hence large amounts of purification, are required, temporal multiplexing will be absolutely essential.

B. Effect of Quantum Memories on Unrestricted Temporal Routing

Although our results are conclusively in favour of temporal multiplexing over spatial multiplexing, and quantum memories will be critical for enabling large amounts of purification, it is not yet clear how critical quantum memories are for mitigating congestion. This is because `QuNet` allows two mechanisms for routing entanglement through time: memory channels and asynchronous links. We quantify the effect of memories by considering the average maximum time-depth reached by our `greedy_multi_path` algorithm for two different 10×10 grid networks: One with no memory channels for routing, and one with additional memories available at each node for routing. Note that the nodes in both networks also each have access to one bit of quantum memory for the purpose of multi-path purification.

If the addition of memory channels improves the efficiency of multipath routing through our network, we expect the average maximum time-depth to be lower in the case where memories are used because of more efficient resource allocation. What we find in Fig. 21, however, is that the memory channels make no significant difference in the maximum time-depths reached in any of the maximum path cases. This means that asynchronous communication along already appears to be sufficient to achieve a minimal time depth for full multipath capacity, and the maximum communication bandwidth for our `greedy_multi_path`

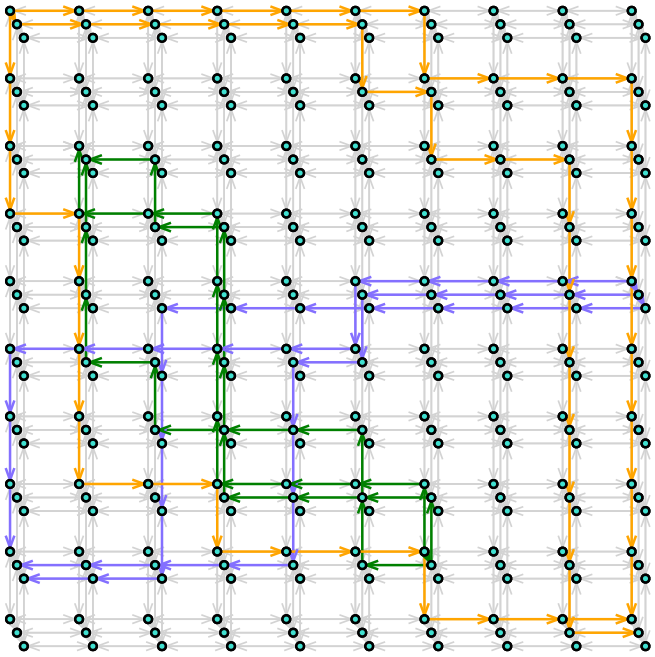

Figure 19: Example of multi-user, multi-path temporal routing with 3 temporal steps (stacked). Utilised channels are colour coded according to which user-pair they serve.

scheme. This therefore suggests that the key benefit of quantum memories for entanglement networking is not to improve the efficiency of multi-path routing, but rather to enable multi-path purification between time layers, and to circumvent the constraints of node connectivity on multipath capacity. Since purification provides asymptotic improvements to fidelity, we conclude that memories will be particularly vital for quantum networks with stringent fidelity requirements.

IX. FURTHER APPLICATIONS

In the previous sections, we validated the performance of `QuNet` for key primitive networking scenarios, and demonstrated how `QuNet` can be used to study complex network features like temporal multiplexing. Here, we conclude with a few brief examples of how `QuNet` can be applied to analyse the performance of networks of real-world significance. Specifically, we explore how to use `QuNet` to determine secret key rates for quantum key distribution (QKD), and determine the bandwidth of above-threshold Bell pairs for fault-tolerant distributed quantum computation. We also demonstrate how `QuNet` could be used as a framework for simulating entanglement distribution satellite networks. Our proof of concept is a cost-evaluation for a simple time-dependent satellite network.

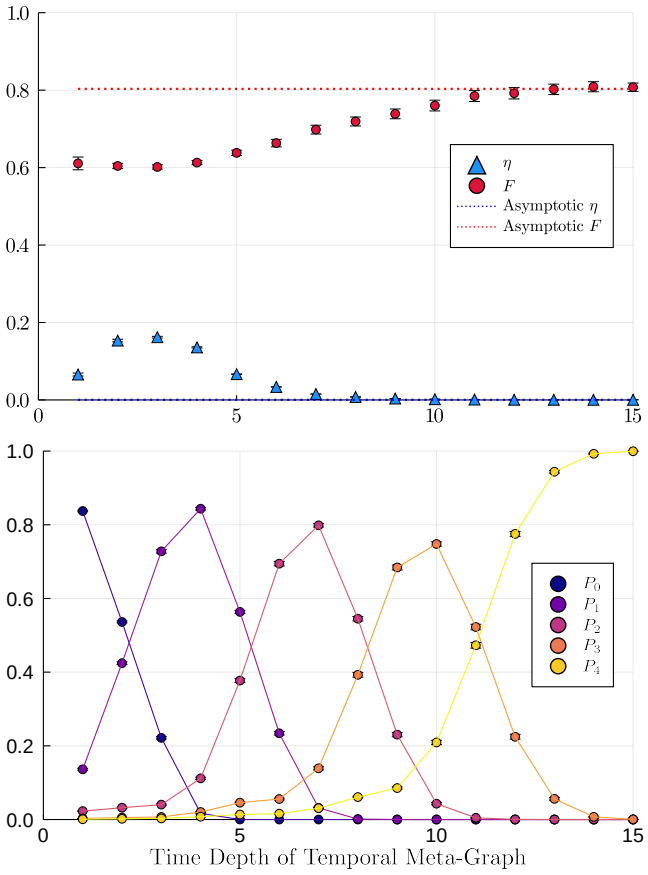

Figure 20: Network performance versus the maximum allowed time-depth. The underlying network is a 10×10 grid lattice that is extended to n distinct temporal layers and 1 asynchronous layer that represents the nodes irrespective of time. Each node is equipped with a lossless quantum memory and so has a directed edge to itself at the next time layer up to the maximum depth. For each sample, a random user pair is chosen at the asynchronous layer and is routed through the temporal network using `greedy_multi_path`. Each edge (Except for those corresponding to lossless memory) has 1dB costs in efficiency and fidelity, and each data point was collected with 1000 samples. (top) Average routing costs in terms of the efficiency η, and fidelity F of the Bell pair. The dotted lines are the costs for η and F in the limit where it is assumed each userpair has a time layer to themselves. (bottom) Probabilities of different path finding scenarios such that P_j is the case that j paths were found between the userpair.

A. Quantum key distribution

The raw mean Bell pair distribution rate for a single user within the network is given by,

$$R_u = \frac{(1 - P_0)\langle \eta \rangle}{\tau}, \tag{9.1}$$

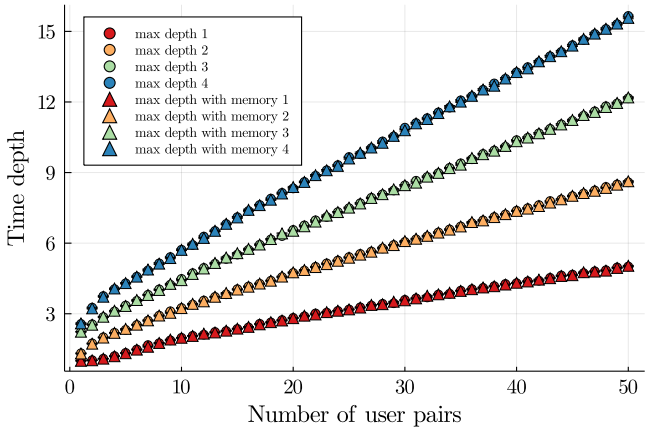

Figure 21: A comparison of the average maximum time depth reached by `greedy_multi_path` for two different networks; Both are 10×10 grids extended in time by 20 layers but one has lossless quantum memories on each node while the other has none. If a node has a memory, there exists a directed edge pointing the node to itself at the next time-layer. The routing between temporal layers is unrestricted, meaning that users may start and finish at any level they like so long as it respects causality. Earlier times are prioritised over later times, and asynchronous routing is prioritised over memory channels. Each edge (Except for those corresponding to lossless memory) has 1dB costs in efficiency and fidelity, and each data point was collected with 1000 samples of randomly chosen user pairs. Data analysis confirmed that the maximum time depth of 20 was never reached in any of the samples.

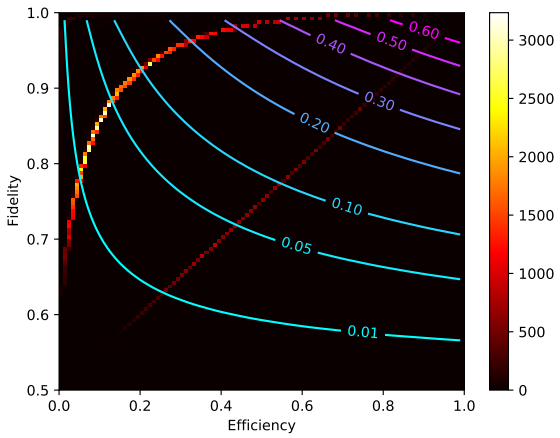

Figure 22: Density heatmap in fidelity/efficiency space of randomly chosen user-pairs in a 100×100 grid network, sampled over 5000 instances of 50 competing user-pairs. A single user-pair contributes a single point in the plane, representing its end-to-end fidelity and efficiency. Superimposed is the tradeoff curve for QKD given by Eq. 9.3, where contour labels denote the secret key rate per user, C.

and the net mean Bell pair rate for the entire network across all users is,

$$\begin{aligned} R_n &= M R_u \\ &= \frac{M(1-P_0)\langle\eta\rangle}{\tau}, \end{aligned} \tag{9.2}$$

where M is the number of user-pairs, P_0 is the probability of no paths being found, $\langle\eta\rangle$ is the average efficiency, and τ the number of time-steps required to route all users (i.e the utilised depth of the temporal meta-graph).

For QKD, the secret key rate (C) is related to the fidelity (F) and raw qubit-rate (R) via, (Nemoto *et al.*, 2016),

$$C = R \cdot [1 - H(\varepsilon)], \tag{9.3}$$

where,

$$H(x) = -x \log_2 x - (1-x)\log_2(1-x), \tag{9.4}$$

is the binary entropy, and the error rate $\varepsilon = 1 - F$. Thus for a given secret key rate we can establish a trade-off curve between the required fidelity and efficiency.

We can visualise the routing costs for a quantum network as a density plot and overlay a contour of curves for different secret key rates, shown in Fig. 22. Each point in the plot represents the fidelity and efficiency achieved by a single user-pair, where the intensity of the point is the relative outcome rate. For a large sample of user-pairs over many trials, such a plot fully captures the scope of the cost-vector distribution of the network.

Visualising network routing costs in the form of a heatmap additionally provides insights into cost tradeoffs across all user-pair configurations in the network. In Fig. 22 we see two dominant curves corresponding to single- and two-path routing. In Fig. 23 we overlay the scatterplot of this data with analytic curves representing competition-free multi-path routing costs for up to four paths. The derivation for these is provided in App. C. Fig. 24 provides deeper insight into the relationship between path utilisation and fidelity/efficiency tradeoffs in a multi-user setting.

B. Distributed quantum computation

A more ambitious and challenging future application for the quantum internet is distributed quantum computation (DQC). The incentive for unifying geographically disjoint quantum computers is far greater than that for conventional classical infrastructure given the superlinear scaling in their computational return upon unification. Furthermore, the prospects of such cloud-based quantum computing are strengthened by the possibility of information-theoretically secure homomorphic encryption (Ouyang *et al.*, 2020; Tan *et al.*, 2016) and blind quantum computing (Broadbent *et al.*, 2009), which are either impractical (in the former case) or impossible (in the latter case) in the classical context.

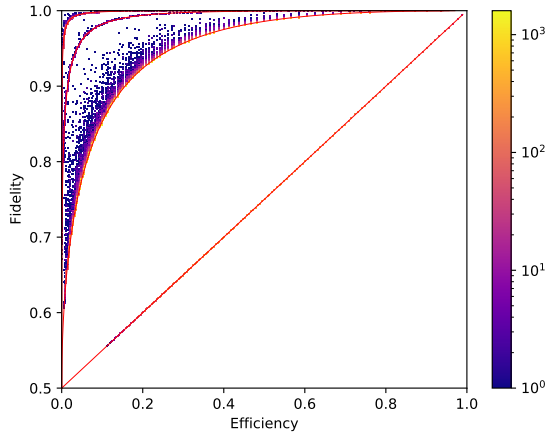

Figure 23: Scatterplot of fidelity/efficiency tradeoffs analogous to Fig. 22, superimposed with the analytic curves (red) derived in App. C. The four red curves show ideal congestion-free tradeoff curves for different numbers of paths utilised in multi-path routing. The blue dots correspond to simulated data points, which deviate from these curves as a result of congestion effects.

For n unified classical computing nodes we expect an $\sim n$-fold gain in their unified computational power. However the computational return on monetary investment is roughly invariant under unification given that n nodes also cost n times as much.

This observation changes in the quantum regime. Considering a quantum algorithm with exponential scaling as an example: When operating independently we make the same observation as before, however when unified the factor of n shifts into the exponent creating a superlinear return on investment. However this can only be realised when the underlying network is also quantum.

A simple model for realising this is in the measurement based model using graph states (Raussendorf and Briegel, 2001; Raussendorf *et al.*, 2003). Where n nodes each to hold a lattice graph state, shared Bell pairs (which are equivalently 2-qubit graph states themselves) can be utilised to mediate fusing them together in a patchwork manner. Now rather than n instances of smaller quantum computers, we have a single one with an n-fold increase in its qubit resources. This concept is shown in Fig. 25.

More precisely, we can quantify this as follows. Let $f_{\mathrm{sc}}(n)$ denote a *computational scaling function* (Rohde, 2021), characterising the net computational power associated with physical computational resources n (measured in say bits, qubits, cores or nodes). Let n_i be the computational resources held by the ith of N nodes. Then the computational advantage provided by networked computational nodes relative to unnetworked nodes is,

$$\lambda = \frac{f_{\mathrm{sc}}\left(\sum_{i=1}^{N} n_i\right)}{\sum_{i=1}^{N} f_{\mathrm{sc}}(n_i)}. \tag{9.5}$$

Considering the case where all nodes have identical resources at their disposal this simplifies to,

$$\lambda = \frac{f_{\mathrm{sc}}(Nn)}{N \cdot f_{\mathrm{sc}}(n)}. \tag{9.6}$$

In the classical case, where $f_{\mathrm{sc}} = n$, we have $\lambda = 1$, whereas in the best case quantum scenario we have $\lambda = O(\exp(N))$. This ratio λ directly relates to the economic incentive to unify remote computational resources, self-evidently far greater in the quantum computational context.

In the context of DQC our requirements are quite different than for QKD, and we might instead consider the rate of pairs above a required fault-tolerance threshold (F_{th}),

$$R_{\mathrm{th}} = R \cdot \mathbb{P}(F \geq F_{\mathrm{th}}). \tag{9.7}$$

This is a quantity which, given a data set for the routed costs, is easy to infer by simply counting the data-points that meet or exceed the required fidelity.

C. Space-based quantum networks

`QuNet` accommodates for dynamic nodes and channels and, in principle, could be used as a high-level tool for simulating and benchmarking entanglement distribution satellite networks. (Yin *et al.*, 2020) In this section, we model a basic satellite network and demonstrate how the costs of distributing entanglement between an end-user pair vary in time. This network is shown in Fig. 26. It consists of two ground nodes and a satellite node that tracks overhead at constant velocity.

Channels $S \leftrightarrow A$ and $S \leftrightarrow B$ are atmospheric free-space links. We employ a simple model for efficiency and fidelity through atmospheric channels, beginning with a model for effective atmospheric depth,

$$\rho(h) = \rho_0 \cdot \exp\left(-\frac{h - h_0}{H}\right), \tag{9.8}$$

where $\rho(h)$ is the atmospheric density at altitude h, and ρ_0 and H characterise density at ground level and the attenuation with altitude. Since the atmospheric density is variable with height, we perform a numerical integral to establish an effective distance d with respect to a standard density,

$$d = \frac{1}{\rho_0} \int_0^L \rho(x \sin\theta)\, dx, \tag{9.9}$$

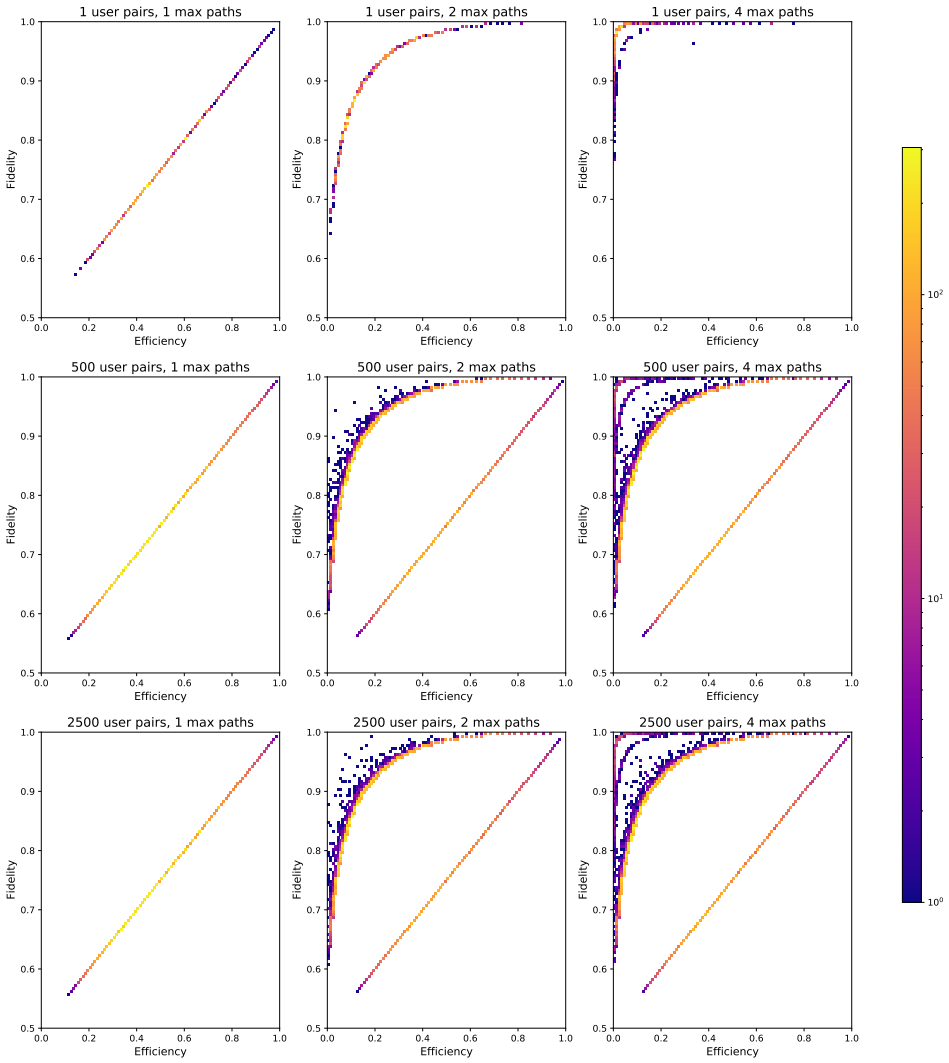

Figure 24: Fidelity/efficiency tradeoff curves for multi-user, multi-path routing. From left to right the subplots correspond to different numbers of maximum allowed paths. From top to bottom we increase the number of competing user pairs.

where L is the Euclidean distance between the ground node and satellite, and θ is the azimuth from ground node to satellite.

With dephasing, we assume an exponential decay in the state fidelity with respect to effective distance, parameterised such that as $d \to \infty$ the state fidelity approaches $\frac{1}{2}$,

$$F = \frac{1 + e^{-\beta d}}{2}. \tag{9.10}$$

For loss, we assume a similar exponential decay associated with atmospheric attenuation, in addition to a quadratic dispersion term,

$$\eta = e^{-\beta d} \cdot \frac{d_0^2}{(d + d_0)^2}, \tag{9.11}$$

where d_0 is a focal length such that $\eta|_{d=0} = 1$.

For the network in Fig. 27, there are three possible ways for the end users A and B to distribute entanglement:

- Via the static channel.

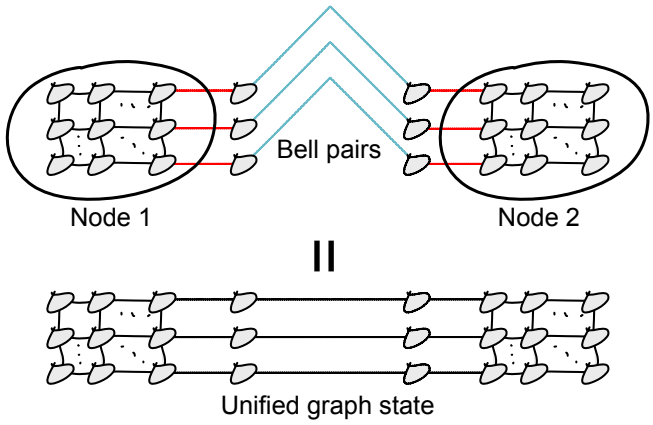

Figure 25: Toy model for distributed quantum computing using graph states. (top) Two geographically separated nodes with local lattice graph states. Distributed Bell pairs (cyan) are equivalently 2-qubit graph states, which may be locally fused onto each of the separated lattices using CZ gates (red). (bottom) The equivalent distributed graph state following entanglement distribution and local fusing operations. These distributed unified graph states have greater computational power than the two individual nodes operating independently, or networked via only classical channels.

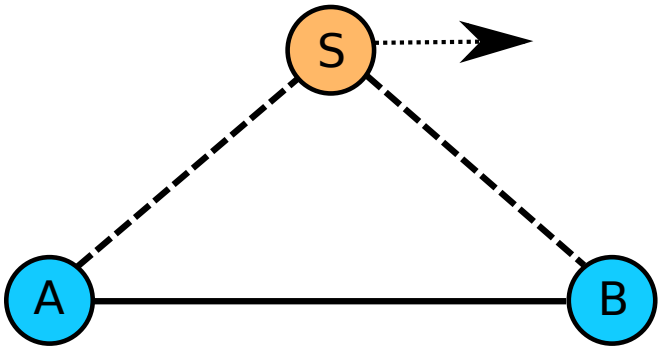

Figure 26: A schematic of the toy satellite network evaluated in Fig. 27. Nodes A and B are fixed communication pairs with a static channel between them. A satellite capable of transmitting entanglement between A and B moves overhead with constant velocity.

- Via the free-space channel.
- Using entanglement purification across both (Sec. II.D).

These are shown in Fig. 27 as the satellite follows its trajectory over time.

As expected from the plot, we see the costs from the free-space channels are minimised when the satellite is directly overhead at $t = 5$. Notice also that the fidelity of the purified route outperforms both of its constituents, but at the expense of higher loss via the non-determinism of the purification protocol. That is, there is a direct trade-off between fidelity (quality) and efficiency (quantity or bandwidth). Though this example is more illustrative

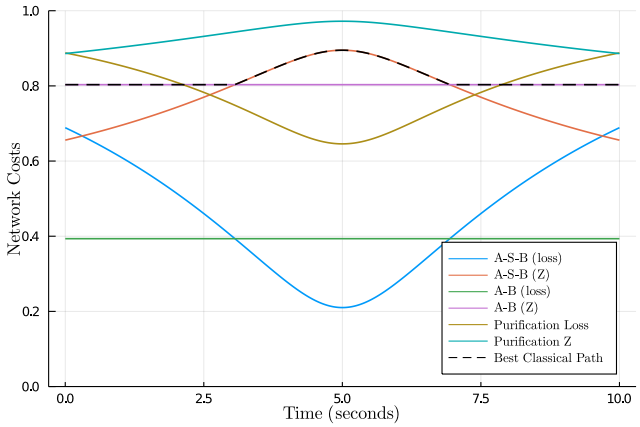

Figure 27: An evolution of the various costs of the distribution methods between end users A and B in Fig. 26. The best available single path in terms of fidelity is given by the black dotted line.

than practical, it can be readily extended to larger scale networks, in particular towards the objective of simulating quantum satellite constellations.

X. CONCLUSION

In this paper we developed a formalism for entanglement distribution quantum networks with Bell pairs as the entanglement resource. We introduced a novel method for quantifying the effects of noisy channels on states with additive cost-metrics thereby making the framework compatible with existing highly optimised shortest-path algorithms. We designed an efficient multi-user, multi-path routing algorithm using greedy iterations of series and parallel graph reductions via entanglement purification and swapping respectively. We also examined the trade-offs between the fidelity and bandwidth that emerge from multi-path routing techniques. Finally to demonstrate our theory, we developed a software package `QuNet` that allows users to simulate time-dependent entanglement networks and benchmark multi-user routing algorithms over an extensive range of applications.

There are many options for further research. In this paper we predominantly considered grid-lattice networks, but one could develop graph topologies that are more optimal for achieving end-user demands. Additional one could study more advanced graph reduction and multi-path routing techniques and benchmark them against the simple greedy case. `QuNet` can also be used as a tool to evaluate infrastructure costs. For example, a quantum satellite constellation could form the backbone for a global quantum network by distributing entanglement between far away ground stations. By simulating such a network with respect to the anticipated demand, one could then put a dollar cost value on the implementation.

"The day science begins to study non-physical phenomena, it will make more progress in one decade than in all the previous centuries of its existence." – Nikola Tesla.

ACKNOWLEDGEMENTS

We thank Darcy Morgan, Alexis Shaw, Marika Kieferova, Zixin Huang, Louis Tessler, Yuval Sanders, Jasminder Sidhu, Simon Devitt & Jon Dowling for conversation (both helpful, unhelpful, meaningless, derogatory, and diatribe). Deepesh Singh was supported by the Australian Research Council Centre of Excellence for Quantum Computation and Communication Technology (project CE110001027). Peter Rohde and Nathan Langford are funded by ARC Future Fellowships (projects FT160100397 and FT170100399, respectively).

Appendix A: Efficient multi-user temporal routing algorithm

Referring to Fig. 13, the temporal meta-graph H can be conceptualised as the direct sum of the planar graphs G representing underlying network, with directed edges between corresponding nodes in the temporal direction.

In the case where all nodes have memory this is equivalent to the Cartesian product of the network graph G and a path graph representing forward time evolution, P_T,

$$H = G \times P_T, \tag{A1}$$

for a time-independent graph G.

Alternately, if no nodes have memory there are no temporal links and we are left with a direct sum of the graphs,

$$\tilde{H} = \bigoplus_{t=1}^{T} G. \tag{A2}$$

Following this, user-pair endpoints are fused to create asynchronous nodes.

The shortest path algorithm is applied to this 3D structure, in which routes can weave both across the planar degrees of freedom and over forward time-steps. So long as a route $A_i \to B_i$ exists in G_i for all i the algorithm is guaranteed to find simultaneous routes for all user-pairs in H, but in general will find more optimal ones than by restricting user-pair i to G_i alone. In the worst case, each user-pair utilises a distinct layer, thus $T = M$. The incrementing multiples of ϵ associated with the edge weights of asynchronous nodes guides the algorithm to prioritise earlier routes, effectively compacting routes in the temporal degree of freedom. Thus, in general $T < M$.

The number of vertices in the temporal meta-graph with asynchronous nodes is given by,

$$\tilde{V} = TV + 2M, \tag{A3}$$

where TV denotes the number of vertices in the T slices of the temporal meta-graph, $2M$ accommodates for the asynchronous nodes, and V denotes the number of vertices in the original (static) graph. Edge weights of the directed vertical temporal channels specify the cost of waiting a single discrete time-step. Thus, the construction allows conflicts between users to be resolved by the shortest path algorithm rather than relying on combinatorics.

The worst-case complexity of performing a single instance of Dijkstra's algorithm on the temporal meta-graph is,

$$O((TV + 2M)^2). \tag{A4}$$

Note that the worst-case scenario for ensuring conflict-free routings between all user-pairs is when each user-pair is forced into a distinct layer of the temporal meta-graph. Thus, T is upper-bounded by M, and Eq. A4 simplifies to,

$$O(M^2V^2). \tag{A5}$$

And to route all M user-pairs via successive applications of Dijkstra's algorithm, the net time-complexity is,

$$O(M^3V^2). \tag{A6}$$

Thus the multi-user shortest-path temporal routing algorithm incurs an M^3 overhead on top of Dijkstra's algorithm and remains a deterministic polynomial-time algorithm.

This technique avoids the exponential overhead associated with naïvely performing combinatoric optimisation over the distinct time-slots designated to each user-pair, for which T^{2M} permutations exist, exponential in the number of users.

It appears that this algorithm is a slightly modified rediscovery of the shortest-path temporal routing algorithm presented by (Kim and Tanchoco, 1991).

This variant has the benefit that the incremental weighting of asynchronous node edges guides the underlying

shortest-path algorithm to preferentially seek the earliest available routing, and the integer multipliers of ϵ specify the time-ordering for each user-pair, implicitly providing the routing queue as an output. Note that ϵ is chosen to be smaller than the smallest edge weight in the graph,

$$\epsilon \ll \min(w(G)), \tag{A7}$$

such that they preferentially guide the algorithm towards the earliest available time-slots without corrupting the identification of which path is shortest (identified shortest path lengths must subsequently be discounted by the appropriate multiples of ϵ).

The maximum index of the traversed nodes provides the worst-case latency experienced by users,

$$\tau = \left\lfloor \frac{\max(\vec{V}_{\text{trav}})}{V} \right\rfloor, \tag{A8}$$

where $\vec{V}_{\text{trav}}$ is the set of traversed nodes within the temporal graph (not including asynchronous nodes), and V is the number of nodes in the original non-temporal graph. This not only acts as an indicator of latency and congestion in the network, but also provides a useful guide for optimising execution time. Specifically, if $\tau < T$ this implies the remaining $T-L$ time-slices are algorithmically redundant for the current problem instance.

The ratio,

$$B = \frac{M}{\tau}, \tag{A9}$$

represents net network bandwidth measured in end-to-end Bell pairs per time-step across the whole network. The theoretical lower bound on this is $B = 1$, corresponding to each user-pair being allocated to a distinct time-step, $\tau = M$. And the theoretical upper bound is $B = M$, when all successfully communicate in a single-shot, $\tau = 1$.

The ratio,

$$R_c = \frac{B(\tilde{H})}{B(H)}, \tag{A10}$$

between the bandwidths with full memory connectivity (Eq. A1) and none (Eq. A2), effectively defines a compression ratio for how much additional bandwidth is enabled by temporal routing through memory channels.

Appendix B: Average L_1-distance between random user-pairs on a square lattice

The number of ways N, to pick two distinct vertices in an $n \times n$ grid lattice is equivalent to the number of ways to pick two distinct pairs of positive integers no greater than n:

$$N \equiv n^2(n^2-1) \tag{B1}$$

The average L_1 distance between two distinct vertices is therefore:

$$\langle L_1 \rangle = \frac{\sum_{x_1,x_2,y_1,y_2}^{n} |x_1 - x_2| + |y_1 - y_2|}{N} \tag{B2}$$

Where $(x_1, y_1), (x_2, y_2)$ are the coordinates of the vertices in the lattice. Expanding the series to separate x and y:

$$\langle L_1 \rangle = \frac{n^2(\sum_{x_1,x_2}^{n} |x_1 - x_2| + \sum_{y_1,y_2}^{n} |y_1 - y_2|)}{N} \tag{B3}$$

$$= \frac{n^2(2\Delta)}{N} \tag{B4}$$

Where

$$\Delta \equiv \sum_{x_1,x_2}^{n} |x_1 - x_2| = \sum_{y_1,y_2}^{n} |y_1 - y_2| \tag{B5}$$

Let $\Delta = \Delta^+ + \Delta^-$ where Δ^+ contains the terms such that $x_2 < x_1$, and Δ^- the ones where $x_1 < x_2$. By symmetry we see that, $\Delta^+ = \Delta^-$. Then,

$$\begin{aligned} \Delta = 2\Delta^+ &= 2\sum_{x_1=1}^{n-1} \sum_{x_2=x_1+1}^{n} (x_2 - x_1) \\ &= \frac{n(n^2-1)}{3}. \end{aligned} \tag{B6}$$

By substitution, we find that

$$\langle L_1 \rangle = \frac{2}{3}n \tag{B7}$$

Appendix C: Derivation of analytic heat map curves

In Fig. 23 of Sec. IX.A, we visualised the routing costs for competing end-users in the form of a heatmap, overlaid with analytic fidelity/efficiency curves for competition-free routing. Here we provide the derivation of these, each corresponding to multipath routing utilising a given number of paths.

Considering a square lattice network with identical channel costs for both dephasing and efficiency, the efficiency and fidelity are related via,

$$F_1 = \frac{1}{2}(E_1 + 1). \tag{C1}$$

The notation (E_1, F_1) denotes the efficiency and fidelity associated with single path routing. Referring to Eq. 2.17 describing the efficiency and fidelity of a purified state,

we use the following recursion relations to establish lower bounds for (E_i, F_i) curves where $1 < i \leq 4$ denotes the number of utilised paths,

$$F_{i+1} = \frac{F_i F_1}{F_i F_1 + (1-F_i)(1-F_1)},$$
$$E_{i+1} = E_1 E_i (F_1 F_i + (1-F_1)(1-F_i)). \quad \text{(C2)}$$

Note that these approximate relationships neglect path competition resulting from multi-path routing (as opposed to competition from other users) and assume all utilised paths are identical. In reality path competition arising from multi-path routing will necessarily extend the length of some paths. Hence these result provide only a lower bound on net cost following purification.

REFERENCES

Bartlett, Ben (2018), "A distributed simulation framework for quantum networks and channels," arXiv:1808.07047 [quant-ph].

Bennett, C H, and G. Brassard (1984), "Quantum cryptography: Public key distribution and coin tossing," Proceedings of the IEEE **1**, 175, arXiv:2003.06557.

Bennett, Charles H, Gilles Brassard, Claude Crépeau, Richard Jozsa, Asher Peres, and William K. Wootters (1993), "Teleporting an unknown quantum state via dual classical and einstein-podolsky-rosen channels," Physical Review Letters **70**, 1895.

Bollobás, Béla, and Oliver Riordan (2006), "Sharp thresholds and percolation in the plane," Random Structures & Algorithms **29**, 524.

Broadbent, A, J. Fitzsimons, and E. Kashefi (2009), "Universal blind quantum computation," in *2009 50th Annual IEEE Symposium on Foundations of Computer Science*, Vol. 50, p. 517, arXiv:0807.4154.

Coopmans, Tim, Robert Knegjens, Axel Dahlberg, David Maier, Loek Nijsten, Julio Oliveira, Martijn Papendrecht, Julian Rabbie, Filip Rozpędek, Matthew Skrzypczyk, Leon Wubben, Walter de Jong, Damian Podareanu, Ariana Torres Knoop, David Elkouss, and Stephanie Wehner (2020), "Netsquid, a discrete-event simulation platform for quantum networks," arXiv:2010.12535.

Dahlberg, Axel, and Stephanie Wehner (2018), "Simulaqron – a simulator for developing quantum internet software," Quantum Science & Technology **4**, 015001, arXiv:1712.08032.

Devitt, Simon J, Andrew D. Greentree, Ashley M. Stephens, and Rodney Van Meter (2016), "High-speed quantum networking by ship," Scientific Reports **6**, 36163, arXiv:1410.3224.

DiAdamo, Stephen, Benjamin Zanger Janis Nötzel, and Mehmet Mert Bese (2020), "Qunetsim: A software framework for quantum networks," arXiv:2003.06397.

Dijkstra, Edsger W (1959), "A note on two problems in connexion with graphs," Numerische Mathematik **1**, 269.

Dür, W, H.-J. Briegel, J. I. Cirac, and P. Zoller (1999), "Quantum repeaters based on entanglement purification," Physical Review A **59**, 169, arXiv:quant-ph/9808065.

Ekert, Artur K (1991), "Quantum cryptography based on bell's theorem," Physical Review Letters **67**, 661.

Fredman, Michael Lawrence, and Robert E. Tarjan (1984), "Fibonacci heaps and their uses in improved network optimization algorithms," in *IEEE 25th Annual Symposium on Foundations of Computer Science*, p. 338.

Gerry, Christopher C, and Peter L. Knight (2005), *Introductory quantum optics* (Cambridge University Press).

Gisin, N, and R. Thew (2007), "Quantum communication," Nature Photonics **1**, 165, arXiv:quant-ph/0703255.

Gouët, Jean-Louis Le, and Sergey Moiseev (2012), "Quantum memory," Journal of Physics B **45**, 120201.

Jian-Wei, Pan, Christoph Simon, Caslav Brukner, and Anton Zeilinger (2001), "Entanglement purification for quantum communication," Nature **410** (6832), 1067–70, copyright - Copyright Macmillan Journals Ltd. Apr 26, 2001; Last updated - 2017-10-31; CODEN - NATUAS.

Kesten, Harry (1982), *Percolation Theory for Mathematicians* (Springer).

Kim, Chang W, and J. M. A. Tanchoco (1991), "Conflict-free shortest-time bidirectional agv routeing," International Journal of Production Research **29**, 2377.

Lvovsky, A, B. Sanders, and W. Tittel (2009), "Optical quantum memory," Nature Photonics **3**, 706, arXiv:1002.4659.

Matsuo, Takaaki (2019), "Simulation of a dynamic, ruleset-based quantum network," arXiv:1908.10758 [quant-ph].

Munro, W J, R. Van Meter, S. G. R. Louis, and K. Nemoto (2008), "High-bandwidth hybrid quantum repeater," Physical Review Letters **101**, 040502, arXiv:0808.0307.

Munro, William J, Koji Azuma, Kiyoshi Tamaki, and Kae Nemoto (2015), "Inside quantum repeaters," IEEE Journal of Selected Topics in Quantum Electronics **21**, 6400813.

Nemoto, Kae, Michael Trupke, Simon J. Devitt, Burkhard Scharfenberger, Kathrin Buczak, Jörg Schmiedmayer, and William J. Munro (2016), "Photonic quantum networks formed from nv-centers," Scientific Reports **6**, 26284, arXiv:1412.5950.

Nielsen, M A, and I. L. Chuang (2000), *Quantum Computation and Quantum Information* (Cambridge University Press).

Ouyang, Yingkai, Joseph Fitzsimons Si-Hui Tan, and Peter P. Rohde (2020), "Homomorphic encryption of linear optics quantum computation on almost arbitrary states of light with asymptotically perfect security," Physical Review Research **2**, 013332, arXiv:1902.10972.

Pan, Jian-Wei, Dik Bouwmeester, Harald Weinfurter, and Anton Zeilinger (1998), "Experimental entanglement swapping: Entangling photons that never interacted," Physical Review Letters **80**, 3891.

Proctor, Timothy J, Paul A. Knott, and Jacob A. Dunningham (2018), "Multiparameter estimation in networked quantum sensors," Physical Review Letters **120**, 080501, arXiv:1707.06252.

Raussendorf, Robert, and Hans J. Briegel (2001), "A one-way quantum computer," Physical Review Letters **86**, 5188.

Raussendorf, Robert, Daniel E. Browne, and Hans J. Briegel (2003), "Measurement-based quantum computation on cluster states," Physical Review A **68**, 10.1103/physreva.68.022312, arXiv:quant-ph/0301052.

Rohde, Peter P (2021), *The Quantum Internet* (Cambridge University Press).

Rohde, Peter P, and Timothy C. Ralph (2006), "Error models for mode mismatch in linear optics quantum computing," Physical Review A **73**, 062312, arXiv:quant-ph/0602004.

Sangouard, Nicolas, Christoph Simon, Hugues De Riedmatten, and Nicolas Gisin (2011), "Quantum repeaters based on atomic ensembles and linear optics," Reviews in Modern

Physics **83**, 33, arXiv:0906.2699.

Sangouard, Nicolas, Christoph Simon, Jiří Minář, Hugo Zbinden, Hugues De Riedmatten, and Nicolas Gisin (2007), "Long-distance entanglement distribution with single-photon sources," Physical Review A **76**, 050301, arXiv:0706.1924.

Sidhu, Jasminder S, and Pieter Kok (2020), "Geometric perspective on quantum parameter estimation," AVS Quantum Science **2**, 014701, arXiv:1907.06628.

Stauffer, D, and A. Aharony (1992), *Introduction To Percolation Theory* (Taylor & Francis).

Tan, Si-Hui, Joshua A. Kettlewell, Yingkai Ouyang, Lin Chen, and Joseph F. Fitzsimons (2016), "A quantum approach to homomorphic encryption," Scientific Reports **6**, 33467, arXiv:1411.5254.

Yin, Juan, Yu-Huai Li, Sheng-Kai Liao, Meng Yang, Yuan Cao, Liang Zhang, Ji-Gang Ren, Wen-Qi Cai, Wei-Yue Liu, Shuang-Lin Li, Rong Shu, Yong-Mei Huang, Lei Deng, Li Li, Qiang Zhang, Nai-Le Liu, Yu-Ao Chen, Chao-Yang Lu, Xiang-Bin Wang, Feihu Xu, Jian-Yu Wang, Cheng-Zhi Peng, Artur K. Ekert, and Jian-Wei Pan (2020), "Entanglement-based secure quantum cryptography over 1,120 kilometres," Nature **582**, 501.